Fuel 317 (2022) 123457

Contents lists available at ScienceDirect

Fuel

journal homepage: www.elsevier.com/locate/fuel

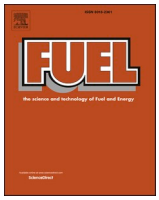

Activity and stability of different Fe loaded primary catalysts for tar elimination

Maria Cortazar [a], Jon Alvarez [b,*], Leire Olazar [a], Laura Santamaria [a], Gartzen Lopez [a,c], Heidi Isabel Villafán-Vidales [d], Asier Asueta [e], Martin Olazar [a]

[a] Department of Chemical Engineering, University of the Basque Country UPV/EHU, P.O. Box 644-E48080, Bilbao, Spain
[b] Department of Chemical and Environmental Engineering, University of the Basque Country UPV/EHU, Nieves Cano 12, 01006 Vitoria-Gasteiz, Spain
[c] IKERBASQUE, Basque Foundation for Science, Bilbao, Spain
[d] Universidad Nacional Autonoma de Mexico, Instituto de Energias Renovables, Temixco, Morelos, Mexico
[e] GAIKER Technology Centre, Basque Research and Technology Alliance (BRTA), Parque Tecnológico de Bizkaia, edificio 202, E-48170 Zamudio, Spain

ARTICLE INFO

Keywords:
Primary catalyst
Biomass gasification
Tar model compound
Tar elimination
Fluidized bed
Catalyst deactivation

ABSTRACT

The performance of olivine, dolomite and γ-alumina primary catalysts was evaluated in the continuous tar elimination process in which toluene was selected as the biomass gasification tar model compound. Iron was incorporated into these catalysts in order to improve their catalytic activity. All the experiments were performed in a continuous flow fluidized bed micro-reactor, with a steam/toluene ratio of 4 and a space velocity (GHSV) of 820 h^{-1}, which corresponds to a catalyst amount of 3.8 cm^3. The effect of temperature was studied using olivine in the 800–900 °C range, which allowed concluding that 850 °C was the best temperature for tar removal. The fresh and deactivated catalysts were characterized by N_2 adsorption–desorption, X-ray fluorescence (XRF), X-ray diffraction (XRD) and temperature-programmed oxidation (TPO). Tar conversion efficiency was assessed by means of carbon conversion, H_2 yield (based on the maximum allowed by stoichiometry), gas composition and product yields, with Fe/Al_2O_3 leading to the highest conversion (87.6 %) and H_2 yield (38 %). Likewise, Fe/Al_2O_3 also provided the highest stability, as it allowed operating for long periods with high conversion values (85.9 % after 35 min on stream), although it underwent severe deactivation. The analysis of the spent catalysts revealed that deactivation occurred mainly by coke deposition on the catalyst surface and iron phase oxidation, with Fe/olivine and Fe/dolomite leading to the faster deactivation due to their poorer metal dispersion related to their reduced surface area. The TPO profiles showed that the coke deposited on the three catalysts was amorphous with a very small contribution of highly structured carbon.

1. Introduction

Biomass gasification is considered one of the most efficient routes to convert biomass feedstock into gaseous fuel through a partial oxidation process at high temperatures [1,2]. However, one of the main shortcomings of biomass gasification lies in the presence of tars in the product stream, which leads to fouling/clogging and corrosion of downstream equipment [3–5]. Hence, in order to minimize the amount of tar and improve the syngas composition, its catalytic conversion is one of most promising routes [6,7]. This process involves the oxidation of the tar components using steam to produce a syngas richer in H_2 and, furthermore, the presence of the catalyst allows a more effective tar removal at lower temperatures than those in the non-catalytic tar conversion [8].

The tar is as a complex mixture of condensable hydrocarbons, ranging from single-ring to five-ring aromatic compounds along with other oxygen-containing hydrocarbons and complex polycyclic aromatic hydrocarbons (PAH) [9]. Tar model compounds have been widely used in order to ascertain the catalyst performance and determine suitable operating conditions. In this work, toluene was selected as a tar model compound because it is a stable aromatic structure, especially at relatively low temperatures, apart from being one of the major tar species in the biomass gasification [10–14].

Many parallel and consecutive reactions involve tar conversion, with the product distribution being the result of their competition. The main products obtained are hydrogen, carbon monoxide and carbon dioxide, and the major reactions occurring in the process are as follows:

* Corresponding author.
E-mail address: jon.alvarezg@ehu.es (J. Alvarez).

https://doi.org/10.1016/j.fuel.2022.123457
Received 23 November 2021; Received in revised form 21 January 2022; Accepted 26 January 2022
Available online 8 February 2022

Toluene steam reforming

$$C_7H_8+7\ H_2O \rightarrow 7\ CO+11\ H_2 \quad (1)$$

Toluene steam dealkylation

$$C_7H_8+H_2O \rightarrow C_6H_6+CO+2\ H_2 \quad (2)$$

Water gas shift (WGS):

$$CO+H_2O \leftrightarrow CO_2+H_2 \quad (3)$$

Thermal cracking

$$C_7H_8 \rightarrow x\ C_nH_m+z\ H_2 \quad (4)$$

$$C_6H_6 \rightarrow x\ C_nH_m+z\ H_2 \quad (5)$$

Hydrodealkylation

$$C_7H_8+H_2 \rightarrow C_6H_6+CH_4 \quad (6)$$

Toluene dry reforming

$$C_7H_8+7\ CO_2 \rightarrow 14\ CO+4\ H_2 \quad (7)$$

Boudouard reaction:

$$C+CO_2 \leftrightarrow 2\ CO \quad (8)$$

Methanation

$$CO+3\ H_2 \leftrightarrow CH_4+H_2O \quad (9)$$

Coke heterogeneous gasification:

$$C+H_2O \rightarrow CO+H_2 \quad (10)$$

Amongst these reactions, the most important ones are steam reforming (Eq. (1)) and water gas shift (WGS) (Eq. (3)).

The selection of temperature and catalyst determines the extent of these reactions and the selectivity towards the different products [7,15–18].

Tar catalytic conversion methods are classified as *in-situ* (or primary) and post-gasification (secondary) ones [14,19]. In the former, the tar reduction occurs during the gasification stage, with the catalyst being located in the gasifier itself. In the secondary approach, the gas produced in the gasifier is treated downstream in a secondary reactor where the catalyst is placed. Regardless the strategy followed, essential aspects conditioning the gasification process are those involving the reactor configuration, operating conditions and type of catalyst [20]. Fluidized bed reactors are one of the most developed technologies for biomass gasification, which require an appropriate catalyst in terms of activity and stability in order to reduce the tar content to 2 g m^{-3} and avoid the need of a more expensive secondary catalytic reactor downstream [21,22].

A wide range of materials with significant activity for cracking and reforming of heavy aromatic compounds have been investigated as primary catalysts [12,14]. Natural minerals, such as olivine and calcined dolomite, have been widely used in the steam gasification in fluidized beds, as they are active for tar removal, apart from being inexpensive and abundant [23]. Acid catalysts, such as alumina or zeolites, have also been used (prior to and after metal impregnation) as catalysts for tar abatement [24]. Nevertheless, the performance of all these primary catalysts can be greatly improved by metal phase addition [19,25–28]. Thus, support features, such as mechanical (resistance to attrition), physico–chemical (surface area, porosity, acidity, composition and density) and catalytic ones (activity / selectivity and stability) play a relevant role in the metal-support interactions, as well as in the reforming reaction mechanism itself [29].

From a catalytic point of view, nickel is known to be the most interesting metal phase for reforming applications [30]. Ni-based catalysts have been widely applied in the steam reforming of biomass tars due to both their high activity for breaking C—C and O—H bonds and performance in terms of H_2 production [7,12,13,31–35]. However, their main drawbacks are related to their rapid deactivation, mechanical fragility and high cost compared to natural minerals or alumina [36]. Currently, use of iron as an active phase is gaining more attention for tar reduction due to its lower cost, abundance and lower toxicity compared to nickel [37]. Iron is known to be an active species for aromatic hydrocarbon destruction (breakage of C—C and C—H bonds), as well as for the WGS reaction. In fact, it has been proven effective for the aforementioned reactions in different oxidation states [24,38–40]. Therefore, iron impregnation of olivine, dolomite or Al_2O_3 seems to be interesting for synthetizing in-bed primary catalysts for gas–solid contact reactors, such as fluidized or spouted beds, from both economic and environmental perspectives. Nevertheless, the lower activity of the iron species with respect to the Ni ones requires higher amounts of dopant, generally in the 10–30 wt% range [41].

Accordingly, the aim of this work is to analyse the performance of olivine, dolomite and γ –Al_2O_3 as primary catalysts, as well as the effect the impregnation of each catalyst with 10 wt% Fe has on the elimination of toluene, which has been selected as the model compound of biomass gasification tar. Furthermore, a detailed characterization of the fresh and deactivated Fe-doped catalysts has been carried out in order to determine the main deactivation mechanisms in this process. The results obtained will provide essential information for the selection of optimal primary catalysts for biomass gasification in the bench-scale unit equipped with an improved spouted bed reactor developed by our research group [21,42,43]. Furthermore, the results obtained may also be extrapolated to industrial gasification reactors, which are mainly fluidized beds. This study addresses multiple aspects that have not been jointly approached in the literature, as are catalysts preparation and characterization, influence of temperature, catalyst performance at zero time on stream, stability of Fe-loaded catalysts and the main deactivation causes.

2. Experimental

2.1. Catalyst preparation and characterization

Six catalysts have been tested in the toluene steam reforming process. Three of them (olivine, dolomite and γ –alumina) are primary catalysts, whereas the other three are those obtained by impregnating the aforementioned primary catalysts with Fe, i.e., Fe/olivine, Fe/dolomite and Fe/Al_2O_3. Besides, runs with silica sand were carried out for comparison purposes. Minerals Sibelco supplied the olivine and dolomite, and Alfa Aesar the γ-Al_2O_3. These three primary catalysts provided satisfactory results in a previous study of biomass gasification in a fountain confined conical spouted bed reactor (CSBR), as they allowed reducing tar formation, as well improving the yield and composition of the syngas [21,42,43]. The catalyst particles were sieved in order to retain the fractions within the ranges of 90–150 μm for olivine, 150–250 μm for dolomite and 250–400 μm for γ - Al_2O_3, which allow attaining similar fluidization regimes with these materials of different densities. Prior to use, dolomite was calcined at 900 °C for 4 h in a muffle oven in order to complete the decarboxylation of calcium and magnesium carbonates.

The Fe loaded catalysts were prepared by wet impregnation of the supports with an aqueous solution of $Fe(NO_3)_3{\cdot}9H_2O$ (Panreac AppliChem, 98 %). The amount of saline precursor added was that corresponding to the desired final catalyst composition. The concentration of Fe was fixed at 10 wt% in order to compare the catalytic activity and selectivity of the three catalysts for same amount of metal loaded. Subsequent to the impregnation process, the prepared catalysts were dried at 100 °C for 24 h and then calcined at 1000 °C for 4 h. Given that the catalytic activity of iron species generally increases with their reduction state (Fe_2O_3 < Fe_3O_4 < FeO < Fe(0)) [26], these iron-impregnated catalysts were used once they had been subjected to an

ex situ reduction process at 850 °C for 4 h under 10 vol% H_2 stream, which ensured full reduction of ferric oxides into their metallic phase. The particle sizes of the Fe loaded catalysts were the same as those of their primary counterparts.

The physical properties of the catalysts were determined by N_2 adsorption–desorption in a Micromeritics ASAP 2010 instrument. Based on the information of these isotherms, the catalysts features, such as those involving specific surface area and porous structure (average pore size and pore volume), were calculated by the Brunauer–Emmett–Teller (BET) method. Prior to the analysis, and in order to remove any impurity, the samples were degassed at 150 °C until a pressure below $2{\cdot}10^{-3}$ mmHg was reached. The chemical composition (wt%) of each catalyst was measured by X-ray fluorescence (XRF). More detailed information about the XRF methodology can be found elsewhere [43].

The temperature-programmed reduction (TPR) of the catalysts was carried out in an AutoChem II 2920 Micromeritics, which allowed determining the catalyst reduction temperature before using it. This method consists in exposing the solid to a reducing gas flow of 10 vol% H_2/Ar, while temperature is increased with a constant heating rate of 5 °C min^{-1} from ambient one to 900 °C. The reduction temperature of each catalyst was ascertained by monitoring the H_2 consumed.

The crystalline structure of the fresh and deactivated catalysts was analyzed using X-ray powder diffraction (XRD) patterns. A Bruker D8 Advance diffractometer with Cu Kα1 radiation was used to conduct XRD. The detailed procedure followed is described elsewhere [44]. The metal crystallite size was calculated by using the Scherrer formula. Metal dispersion was calculated from metal crystallite size using the equation D (%) = 97.1/d (nm) and assuming that the size of Fe atom is the same as that of Ni atom, as reported elsewhere [45,46].

The values of total acidity of the catalysts have been obtained by monitoring the differential adsorption of NH_3 at 150 °C using simultaneously calorimetry and thermogravimetry in a Setaram TG-DSC 111 equipment.

The amount of coke deposited on the used catalysts was determined by temperature-programmed oxidation (TPO) in a thermobalance (TGA Q5000TA Thermo Scientific). This TGA is connected on-line to a Blazer Instruments Mass Spectrometer (Thermostar) and the procedure followed to determine the coke deposited on each sample is as follows: (i) signal stabilization with He stream at 100 °C for 30 min, and (ii) a ramp of 5 °C min^{-1} to 800 °C in a stream of O_2 diluted in He, with this temperature remaining constant for 30 min in order to ensure full coke combustion.

2.2. Experimental equipment and procedure

The experiments of toluene conversion with the different catalysts were performed in an *Inconel* fluidized bed reactor (300 mm in length and 10 mm in internal diameter), as shown in Fig. 1. The reactor is located within a radiant oven, which provides the heat for operating up to 900 °C. The temperature was measured and recorded by means of two K-type thermocouples, with one being located inside the reactor, approximately in the middle zone of the bed, and the other one close to the wall of the electric oven.

The water for generating the steam and toluene were introduced by means of a high-pressure pump (*ASI 521*) and a syringe pump (*PHD 4400*), respectively. Their pumping flowrates were maintained constant in all the runs, with the values being 0.24 mL min^{-1} for water and 0.06 mL min^{-1} for toluene, which correspond to a steam/toluene ratio (S/T) of 4 and a molar steam/carbon (S/C) ratio of 3.35. Prior to feeding into the reactor, these two compounds were pumped separately into an evaporation system at 350 °C, which ensures their full vaporization. This plant is also provided with a nitrogen mass flow meter (*Brooks SLA5800*) that allows feeding up to 1 L min^{-1}. In fact, a nitrogen flow rate of 300 mL min^{-1} was used as fluidizing agent during the heating process prior to the reaction.

The gaseous stream leaving the reactor was passed through a heater, whose temperature was kept at 300 °C in order to prevent the condensation of the products before entering the on-line analysis system. Then, the volatile stream circulated through a condensation device consisting of two coalescence filters, which ensured total condensation and retention of the non-reacted steam and toluene, as well as toluene derived products.

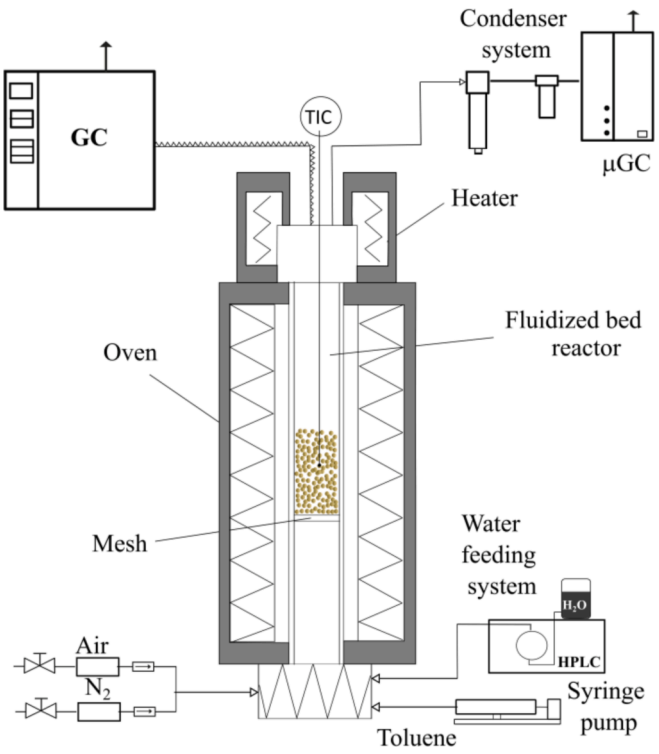

Fig. 1. Schematic diagram of the toluene steam reforming laboratory unit.

This study deals with the effect of operating conditions in a catalytic process for tar elimination process, i.e., reforming temperature (in the 800–900 °C range), catalysts type (olivine, dolomite and alumina, as well as their counterparts with Fe impregnation) and catalyst stability. Olivine was chosen to analyse the effect of temperature, whereas 850 °C was established as the suitable operating temperature to study the influence of catalyst type and time on stream. The effect of reaction time was studied for the Fe loaded catalysts in the 5–115 min range in order to assess the evolution of catalyst activity and stability.

Given that the density of the primary catalysts differs significantly (3300 kg m^{-3} for olivine, 1666 kg m^{-3} for alumina and 1275 kg m^{-3} for dolomite), and in order to operate under the same hydrodynamic conditions in the fluidized bed reactor, the same bed volume was used in all experiments. Accordingly, as mentioned above, suitable particle sizes were chosen. Thus, 3.8 cm^3 of the corresponding catalyst (or sand in case the experiment was carried out without catalyst) were placed in the bed in all cases, corresponding to a gas hourly space velocity (GHSV) of 820 h^{-1}. Experiments at zero time on stream were repeated at least 3 times to ensure reproducibility of the results and the carbon mass balance closure was above 95 % in all runs.

2.3. Product analysis

The analysis of the volatile stream leaving the reactor was conducted on-line by means of a GC (Agilent 7890) provided with a flame ionization detector (FID). The sample was injected into the GC prior to condensation by means of a line maintained at 280 °C in order to avoid the condensation of heavy tar compounds. The analysis of the non-condensable gases (after separating the tars from the gaseous stream in the condensation system) was carried out by means of a micro GC

Table 1
Properties of primary and Fe impregnated catalysts.

	Olivine	Fe/Olivine	γ-Al_2O_3	Fe/Al_2O_3	Calcined Dolomite	Fe /Dolomite
Physical properties						
S_{BET} (m^2 g^{-1})	1.92	3.75	100.00	12.48	17.42	3.55
V_{pore} (cm^3 g^{-1})	0.002	0.017	0.42	0.059	0.05	0.009
d_{pore} (Å)	78	234	167	206	113	162
Chemical properties						
MgO (wt%)	48.79	36.98	–	0.23	43.61	32.15
SiO_2 (wt%)	43.18	37.20	0.02	–	0.12	0.11
Fe_2O_3 (wt%)	7.68	24.39	–	14.13	0.02	13.21
CaO (wt%)	0.12	0.17	–	0.14	56.07	48.53
Al_2O_3 (wt%)	0.04	0.43	99.98	81.02	0.15	0.26
Na_2O (wt%)	0.06	0.06	–	–	0.01	0.03
TiO_2 (wt%)	0.02	0.03	–	0.12	0.02	0.03
MnO (wt%)	0.11	0.10	–	–	–	–
Acidity						
Total acidity (μmol NH_3 g_{cat}^{-1})	2.4	8.8	80.0	11.4	8.7	10.5

(Agilent 4900). The three independent modules with different columns (molecular sieve, porapak and plot alumina) allowed identifying and quantifying the gaseous products previously calibrated. This analysis methodology allowed a detailed quantification of the entire product stream.

2.4. Reaction indices

The conversion and product yields were taken as reaction indices to monitor and assess process performance. The carbon conversion of toluene was defined as the moles of carbon in the gaseous product stream divided by the moles of carbon in the toluene feed (Eq. (11)). Note that the moles of CO, CO_2 and C_1-C_4 hydrocarbons formed (corresponding to the total amount of carbon moles in the gas) have been determined from the micro-GC analysis, whereas the moles of carbon in the feed were calculated based on the total amount of toluene introduced into the reactor (total volume of toluene injected in the run).

$$C_{conversion}(\%) = \frac{moles\ of\ carbon\ in\ the\ product\ gas}{moles\ of\ carbon\ in\ the\ feed} \cdot 100 \quad (11)$$

The product yields were calculated as the ratio between the grams of each product (H_2, CO, CO_2 and CH_4) in the gaseous stream and the grams of the model compound in the feed:

$$Yield(wt\%) = \frac{g\ of\ the\ compound\ in\ the\ product\ gas}{g\ of\ model\ compound\ in\ the\ feed} \cdot 100 \quad (12)$$

Moreover, H_2 potential was also determined as the ratio between the concentration of H_2 in the effluent gas and the maximum allowed by stoichiometry:

$$H_2\ potential(\%) = \frac{moles\ of\ H_2\ in\ the\ product\ gas}{maximum\ moles\ of\ H_2\ allowed\ by\ stoichiometry} \quad (13)$$

The maximum number of H_2 moles allowed by stoichiometry was calculated by considering toluene reforming reaction and that of WGS. Thus, H_2 potential is defined based on the maximum number of H_2 moles obtained when toluene is fully reformed to CO_2 and H_2.

3. Results and discussion

3.1. Fresh catalyst characterization

Table 1 shows the physical properties (specific surface area, pore volume and average pore diameter) and chemical composition of the primary catalysts and those impregnated with Fe. As observed, olivine has the lowest specific surface area (1.92 m^2 g^{-1}) and pore volume (0.002 cm^3 g^{-1}) due to its non-porous structure. After impregnation with $Fe(NO_3)_3{\cdot}9H_2O$ solution, the specific surface area and the pore volume of dolomite and Al_2O_3 decreased mainly due to metal deposition, as it blocks some of the micropores of the catalysts. According to Kumar et al. [47], the presence of iron on alumina accelerates the shrinkage of alumina and transforms the alumina from gamma into other phases, which decreases the surface area because Fe_2O_3 particles act as heterogeneous nucleation sites for α-Al_2O_3 particles at high temperature. Nevertheless, the opposite trend was observed in the Fe/olivine, i.e., the specific surface area increased due to the deposition of Fe on the external surface area, and the pore volume and average pore size became larger, which suggests the collapse of the inter-pore structure of olivine. Note that the same trend has been observed for metal impregnation on supports with low porosity surfaces [22,48,49]. Apart from the impregnation process, the high calcination temperature also contributes to reducing the BET surface area and porosity of the Fe/Al_2O_3 catalyst, although to a lesser extent. In a previous study [50], the same Al_2O_3 used in this study was calcined with air at 1000 °C during 5 h and its BET surface area and pore volume reduced to 87 m^2 g^{-1} and 0.38 cm^3 g^{-1}, respectively.

Dolomite is a calcium magnesium carbonate, i.e., $CaMg(CO_3)_2$, and therefore carbonates are decomposed into CaO and MgO in the calcination, which are the main constituents in the calcined dolomite, as shown in Table 1. Moreover, the XRF revealed that there is a high content of Fe in the Fe/olivine. In fact, the content of Fe in the raw olivine was of around 5.3 wt% and after impregnation, the Fe amount in the catalyst increased significantly to 17 wt%, which confirmed that the metal content was close to that corresponding to the impregnation (~10 wt%) plus that in the original olivine. In the other two catalysts, namely Fe/Al_2O_3 and Fe/dolomite, the initial Fe content was negligible and after the impregnation increased up to 9.9 and 9.3 wt%, respectively. Thus, the Fe content of the three studied catalysts is consistent with the targeted metal loading of 10 wt%.

Table 2 shows the metal dispersion of each catalyst which was estimated based on the metal crystallite size obtained by XRD analysis (by applying Debye-Scherrer equation). As observed, the highest metal dispersion is attained for Fe/Al_2O_3 (2.6 %), whereas the poorest value is for dolomite (0.5 %). This result confirms that the physical structure of the support plays an essential role in the dispersion of the metal phase; that is, the support with the highest surface area as that of Al_2O_3 leads to the highest metal dispersion.

Table 2
Metal dispersion (%) calculated from metal crystallite for the three Fe impregnated catalysts.

	d_{Fe} XRD[a] (nm)	Fe dispersion (%)
Fe/Al_2O_3	38	2.6
Fe/olivine	68	1.4
Fe/dolomite	193	0.5

[a] Calculated from the full width at half height of the Fe^0 (1 1 0) diffraction peak at $2\theta = 44°$ in the XRD profiles using the Scherrer equation.

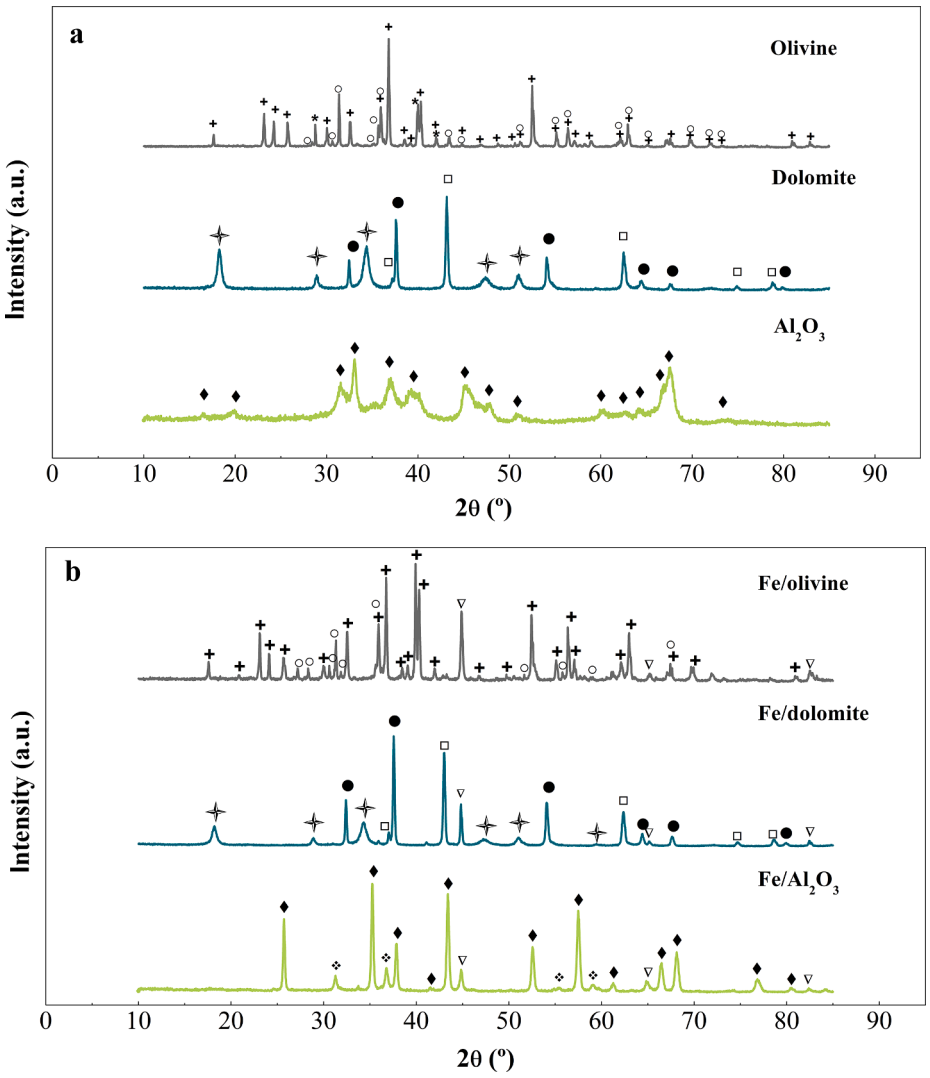

Fig. 2. XRD patterns of primary catalyst (a) and Fe impregnated ones (b). Crystalline phases: (+) ($Mg_{1.81}Fe_{0.19}(SiO_4)$); (o) Enstatite ($MgSiO_3$); (▽) Fe^0; (◆) Al_2O_3; (□) MgO; (●) CaO; (❖) Hercynite ($FeAl_2O_4$); (✦) Calcium hidroxide ($CaOH_2$).

The XRD patterns of the primary catalysts and Fe reduced catalysts are shown in Fig. 2a and 2b, respectively. As observed, the three Fe doped catalysts show an intense peak of the metal iron phase at 2θ = 44° and two smaller ones at 2θ = 65° and 82°. Note that iron oxide phases were not detected in these catalysts, which is evidence of their full reduction. In both olivine (Fig. 2a) and Fe/olivine (Fig. 2b), the main crystalline phases observed are those corresponding to olivine ($Mg_{1.81}Fe_{0.19}·(SiO_4)$) and enstatite ($MgSiO_3$). Further diffractogram of unreduced Fe/olivine catalyst can be found elsewhere [22]. Regarding Fe/dolomite (Fig. 2b), apart from the metal iron phase, those of Ca $(OH)_2$, CaO and MgO were also observed, with all of them being derived from the calcination of calcium magnesium carbonate, which is the main mineral species in the dolomite [51]. These last three phases ($Ca(OH)_2$, CaO and MgO) were also observed in the XRD diffractogram of calcined dolomite (Fig. 2a). These alkaline earth oxides (CaO and MgO) containing Lewis basic sites may promote adsorption and migration of H_2O and OH groups on the catalyst surface, and therefore promote carbon gasification and reduce carbon deposition [52]. The $Ca(OH)_2$ diffraction peaks are evidence that CaO (a highly hygroscopic compound) absorbed humidity from the ambient and formed $Ca(OH)_2$. In the Fe/Al_2O_3 catalyst, typical diffraction peaks corresponding to the Al_2O_3 support were detected, as well as hercynite ($FeAl_2O_4$), whose diffraction lines are located at 2θ = 31°, 36°, 51°, 59° and 64°. The high calcination temperature used (1000 °C) allowed the formation of hercynite spinel ($FeAl_2O_4$), which occurs at temperatures above 600 °C by the interaction between Fe species (Fe^0, FeO and Fe_3O_4) and Al_2O_3, following the reaction mechanism reported in the literature [53,54]. Moreover, comparing the XRD patterns of Al_2O_3 before and after impregnation and calcination stages, there is a phase change from γ-Al_2O_3 to a more stable one, which is probably the most stable one (α-phase) due to the high temperature of calcination used (1000 °C). The peaks assigned to Al_2O_3 in the Fe loaded catalyst in Fig. 2b are clear and sharp, which is evidence of its high crystallization degree, whereas the peaks assigned to Al_2O_3 in Fig. 2a are broad and low, thereby suggesting an amorphous structure with a small crystallization degree. Note that the same diffraction peaks than those observed for Al_2O_3 crystalline phases in Fig. 2a and b have been reported in the literature and correspond to γ-Al_2O_3 and α-Al_2O_3, respectively [55,56]. Therefore, phase transformation is the consequence of the thermal degradation of the support, which affects adversely the physical properties of the catalyst by reducing catalyst surface area, thereby reducing catalyst activity. Several authors have called this process support sintering [35,57].

The temperature programmed reduction (TPR) profiles of calcined Fe/olivine, Fe/dolomite and Fe/Al_2O_3 catalysts are shown in Fig. 3. Given that metal iron is expected to be the active phase for breaking C—C and C—H bonds [24,58], the reducibility of the catalysts is of great

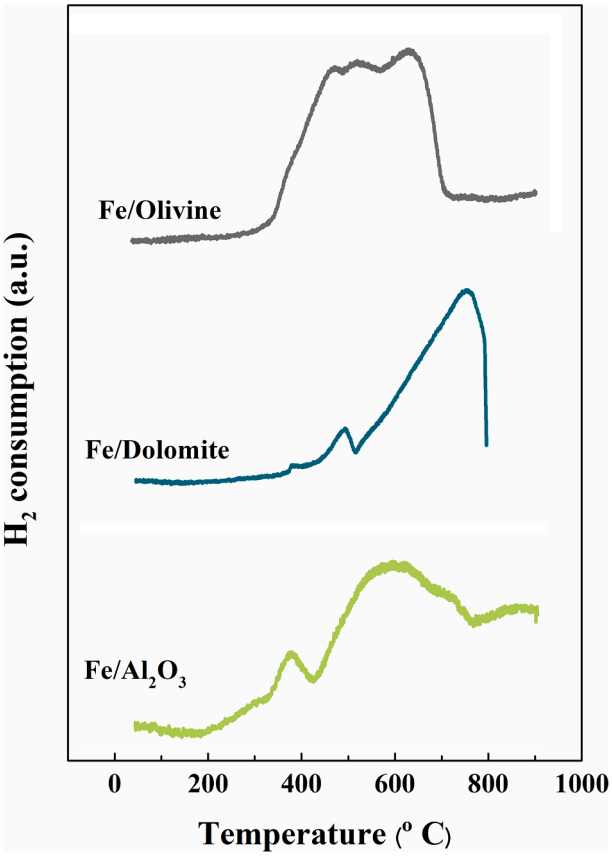

Fig. 3. TPR profiles of Fe/Al_2O_3, Fe/dolomite and Fe/olivine catalysts.

relevance. According to the literature [26,59] the reduction of Fe_2O_3 generally proceeds in two steps, as are: the reduction of Fe_2O_3 to Fe_3O_4 in the 350–500 °C range and the reduction of Fe_3O_4 to metal Fe in the 500–900 °C range. However, according to certain studies, the intermediate FeO is formed in the reduction from Fe_3O_4 to Fe^0 [60,61]. These two regions associated with two or three reduction steps from Fe_2O_3 are observed in the three reduced catalysts, although differences in the interactions between the iron and the supports shifted the location of the peaks. In the TPR profile of the Fe/olivine, a broad reduction zone between 350 and 700 °C is observed with 3 peaks. The first two (at 470 and 530 °C) are associated with the reduction of Fe_2O_3 and Fe_3O_4/FeO, respectively, whereas the latter peak above 600 °C is due to the Fe atoms that migrated into the olivine support to form a very stable $MgFe_2O_4$ spinel phase [62]. Peaks at 380 °C and 500 °C appear in the Fe/dolomite, which are characteristic of iron species reduction, but there is also a broad peak at 750 °C, which corresponds to the reduction of Fe^{3+} from the calcium iron oxide (srebrodolskite, $Ca_2Fe_2O_5$) to Fe, as was suggested by Zamboni et al. [63,64]. These authors observed the formation of this phase when iron nitrate was used in the wet impregnation of dolomite. In this study, no evidences of $Ca_2Fe_2O_5$ are observed in the XRD diffractogram (Fig. 2), probably due to its low crystallinity. In the Fe/Al_2O_3 catalyst, apart from the two peaks identified at 380 and 580 °C, which are associated with the reduction of iron species (Fe_2O_3, Fe_3O_4 and FeO) , a third broad reduction zone appears between 700 and 900 °C, which is attributed to the reduction of iron aluminates ($FeAl_2O_4$), also identified in the XRD spectra [65]. Different authors suggested that the presence of alumina stabilizes Fe_2O_3 phase and the reduction goes through the formation of $FeAl_2O_4$ spinel, whose reduction occurs above 700 °C [66,67].

3.2. Role of temperature in the tar conversion on olivine catalyst

The influence of temperature on toluene abatement on olivine catalysts is displayed in Fig. 4. Fig. 4a shows the evolution of carbon conversion and H_2 potential. As observed, temperature has a great influence on carbon conversion and H_2 potential, since their values increase from 3.6 and 2.6 % at 800 °C to 46.0 and 23.6 % at 900 °C, respectively. This increase in both parameters is attributed to the endothermic nature of the toluene reforming reactions, as well as of those involving decomposition and dehydrogenation, as all of them are promoted at high temperatures [68]. The same trend of carbon conversion and H_2 potential with temperature on olivine catalysts was observed by other authors in the tar steam reforming [58,69].

The yields of the compounds in the product stream is displayed in Fig. 4b. An increase in temperature leads to higher yields in gaseous compounds (including benzene) due to the promotion of both reforming and cracking reactions, with the highest yields being those of CO and CO_2 at 900 °C (49.8 and 26.8 wt%, respectively). The yield of CH_4 increases with temperature, but it is lower than 2.2 wt% at the three temperatures studied. It should be noted that the yield of C_2-C_4 hydrocarbons is hardly noticeable (below 0.01 wt%), and has not therefore been included in Fig. 4b. CH_4 is mainly formed from dealkylation of the methyl group in the toluene structure and, to a minor extent, from the methanation of CO [8]. However, steam reforming of CH_4 prevails over these reactions, since the content of CH_4 in the products is very low [12]. The presence of an undesired compound (benzene) is due to incomplete decomposition of toluene [70], which is confirmed in Fig. 4b, where benzene yield increases from 0.6 wt% at 800 °C to 12.6 wt% at 900 °C at the expense of a decrease in toluene yield. Several reactions, such as steam dealkylation (Eq. 2), thermal cracking (Eqs. 4–5) or hydrodealkylation of toluene (Eq. 6) lead to the formation of benzene (all of them enhanced at high temperatures) [11,15,17,71]. However, the small amount of CH_4 in the product stream is evidence that hydrodealkylation reaction (Eq. 6) is not significant [72]. It should be noted that the benzene produced from the aforementioned reactions can undergo reforming reactions to produce further CO and H_2, although these reactions are limited due to benzene stability [11,12]. The yield of polycyclic aromatic hydrocarbons (PAHs, referred to the compounds heavier than toluene) also increases with temperature due to the promotion of condensation reactions of lighter tars. However, the low yield of these PAHs (below 1.2 wt% in the whole range of temperatures studied) is evidence that the extent of these reactions is almost negligible, probably due to the presence of steam [21,73]. Swierczynski et al. [3] also observed a yield of around 6 wt% of benzene and 14 wt% of polyaromatics in the product stream of toluene steam reforming at 850 °C when they used olivine as primary catalyst.

Fig. 4c displays the gas composition in the 800–900 °C range. It can be observed that the effect of temperature on the gas composition is not very pronounce above 850 °C, i.e., the concentration hardly changes above this temperature. Between 800 and 850 °C, certain trends are observed when temperature is increased, as are: a slight decrease in H_2 and CO_2 concentrations (from 69.1 to 66.2 vol% and from 8.1 to 6.8 vol %, respectively) and an increase in that of CO (from 21.8 to 25.5 vol%). This result is explained by the promotion of the reverse WGS reaction due to its exothermic nature. The same trend with temperature was observed in other studies of catalytic reforming of tar model compounds, with this effect being attributing to the exothermic nature of the WGS reaction [68,74].

3.3. Comparison of primary catalysts performance

In order to study the performance of primary catalysts, toluene conversion on olivine, dolomite and alumina was monitored at 850 °C and the results obtained are displayed in Fig. 5. The effect of thermal cracking was ascertained by comparing the results of carbon conversion (Fig. 5a), product yields (Fig. 5b) and concentration of gaseous

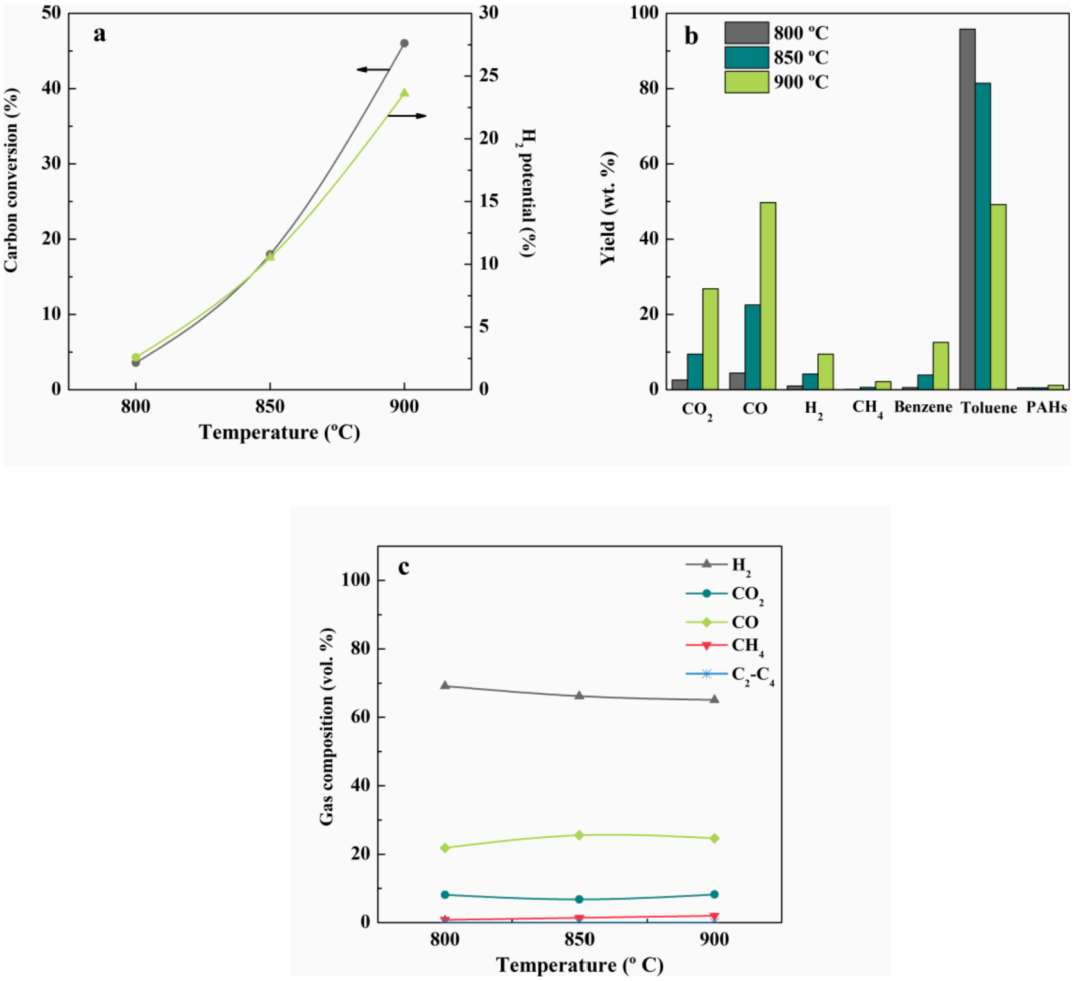

Fig. 4. Effect of temperature on carbon conversion and H_2 potential (a), product yields and unreacted toluene fraction in the outlet stream (b), and concentration of the gaseous stream (c).

compounds (Fig. 5c) obtained with the catalysts and those obtained with inert sand. As observed, the presence of any catalyst improves the overall efficiency of the process by increasing carbon conversion and the yields of gaseous compounds, especially those of H_2, CO and CO_2, as well as reducing that of toluene. This improvement over the results obtained with inert sand is associated with the promotion of steam reforming (Eq. 1), cracking (Eqs. 4–5) and WGS reactions (Eq. 3). The presence of primary catalysts also promotes steam dealkylation (Eq. 2) and thermal cracking (Eq. 4) reactions, since the concentration of benzene in the product stream is higher than that obtained with sand.

Comparing the efficiency of the primary catalysts (Fig. 5a), Al_2O_3 leads to the highest conversion (58.4 %) followed by dolomite (39.1 %). However, the H_2 potential with both catalysts is similar (28.5 % for Al_2O_3 and 28.9 % for dolomite). This latter result can be explained by the lower activity of Al_2O_3 and the higher of dolomite in the WGS. Thus, the higher activity of dolomite in the WGS reaction is related to CaO and MgO basic sites, with activity being higher as the Ca/Mg ratio is increased [75,76]. Furthermore, the presence of CaO and MgO also explains the higher yield of benzene at the expense of lowering that of toluene [77,78]. Moreover, olivine has the smallest influence on the toluene steam reforming, since it provided the lowest carbon conversion and H_2 potential values. In this case, although the presence of Fe promotes reforming reactions, the low BET surface area (1.91 $m^2\ g^{-1}$) and pore volume (0.002 g cm^{-3}) are the factors leading to the low efficiency of this catalyst in the toluene elimination process. Studies reported in the literature confirm that dolomite and Al_2O_3 were more active than olivine for reducing the amount of tar derived from biomass gasification, as the extent of the WGS reaction is enhanced with dolomite [43,79].

3.4. *Effect of Fe incorporation into the primary catalysts*

Fig. 6 compares the parameters involving toluene conversion (carbon conversion and H_2 potential (a), product yields in the outlet stream (b) and the concentration of gaseous compounds (c)) for the Fe loaded catalysts. Fig. 6a reveals that Fe incorporation into the primary catalysts leads to higher carbon conversion and H_2 potential than those on the primary catalysts in all cases, Fig. 5a, which is evidence of their higher catalytic activity for toluene reforming. Thus, on the one hand, it is well stablished that metal iron is active for C—C and C—H bond breakdown, which enhances hydrocarbon reforming and cracking reactions [58,80]. On the other, the addition of Fe promotes the WGS reaction because the adsorption of water molecules on the catalyst active sites is favoured, thus leading to higher H_2 yields [81]. This improvement is especially remarkable with olivine, whose carbon conversion and H_2 potential increases from 18 and 10.5 % to 73 and 31.9 %, respectively.

As occurred with primary catalysts, that of Fe/Al_2O_3 provided the best results in terms of carbon conversion (87.6 %) and H_2 potential (38 %) (Fig. 6a). However, the trends were reversed for Fe/olivine and Fe/dolomite after Fe incorporation, attaining higher carbon conversion in the former. This result is closely related to the change in the surface area of the catalysts caused by the impregnation, which definitely affects metal dispersion. As observed in Table 1, the surface area increased in the olivine when Fe was introduced, whereas it significantly decreased in the dolomite (from 17.42 to 3.55 $m^2\ g^{-1}$). Furthermore, the results in

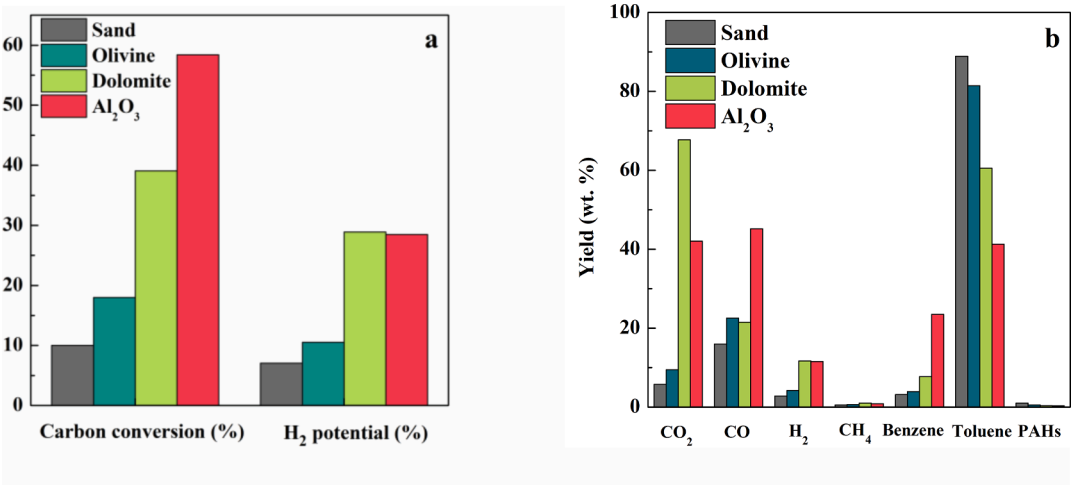

Fig. 5. Effect of primary catalysts on carbon conversion and H_2 potential (a), product yields and unreacted toluene fraction in the outlet stream (b), and concentration of gaseous compounds (c).

Table 2 confirm the better dispersion of Fe on the olivine than on the Fe/dolomite, which suggests that the active sites are more accessible for the reactants in the former, as all the iron is located on the catalyst surface. This implies a higher catalytic activity of Fe/olivine, which explains the better results of carbon conversion on this catalyst than on Fe/dolomite, whose metal dispersion is the poorest.

Comparing the product yields shown in Fig. 6b, the highest yields of CO and CO_2 (mainly derived from the reforming and WGS reactions, respectively) and benzene (a cracking product) are obtained on the Fe/Al_2O_3 catalyst, whereas that of toluene is the lowest (below half of those obtained on Fe/olivine or Fe/dolomite). Note that Fe acts as the active phase for the reforming and WGS reactions, whereas the alumina support provides the acidity required for cracking reactions, i.e., the combination of both provides Fe/Al_2O_3 catalyst with the highest activity for these reactions. Moreover, a comparison of Fig. 6b with Fig. 5b shows that the yield of benzene increases greatly when Fe is added to the primary catalysts. It seems that the presence of Fe mainly catalyzed the conversion of toluene to benzene. Some studies suggested that temperatures higher than 800 °C increase the hydrodealkylation activity for the steam reforming of toluene on iron-based materials [72,82], whereas other researches concluded that the activity of iron-based materials leads to the decomposition of large tar compounds into small fragments of carbon species, which subsequently form benzene [83]. Therefore, it can be concluded that the higher benzene content is a combined effect of cracking and hydrodealkylation of toluene molecules on Fe active sites. The higher CH_4 yields observed on Fe loaded catalyst than on primary catalysts also confirms this hypothesis.

Fig. 6c displays the gas composition obtained with the three Fe-impregnated catalysts. A comparison of these results with those for primary catalysts (Fig. 5c) shows the relevance of metal iron in the WGS reaction (Eq. 3), since the concentration of CO_2 greatly increased in all the cases, whereas that of CO reduced. This is consistent with previous studies in the literature, in which a high activity of Fe is reported in the WGS reaction [38,40,84]. Analysing Fe loaded catalysts, Fe/Al_2O_3 led to the lowest concentration of CH_4 and CO_2 and the highest of H_2 and CO, which is evidence of a high extent of steam and dry reforming of hydrocarbons (Eq. 1 and 7). According to Adnan et al. [85,86], this fact is attributed to the basic sites of Fe/Al_2O_3 catalysts, which promote endothermic CO_2 reforming of hydrocarbons.

The differences observed among these Fe-impregnated catalysts are the consequence of various factors. As previously stated, one of the most influential factor is related to the metal dispersion on the catalyst support, which plays a key role in the initial catalyst activity. A suitable metal-support interaction enhances the migration of metal crystallites, thereby obtaining a better dispersion of Fe on the support [26]. Furthermore, the physical structure of the support greatly influences the dispersion of the metal phase, as shown in Table 2, in which the highest Fe dispersion was obtained for Al_2O_3 (the support with the highest BET surface area and pore volume). The results in Fig. 6 confirm that the better surface properties of the Al_2O_3 support promote the dispersion of

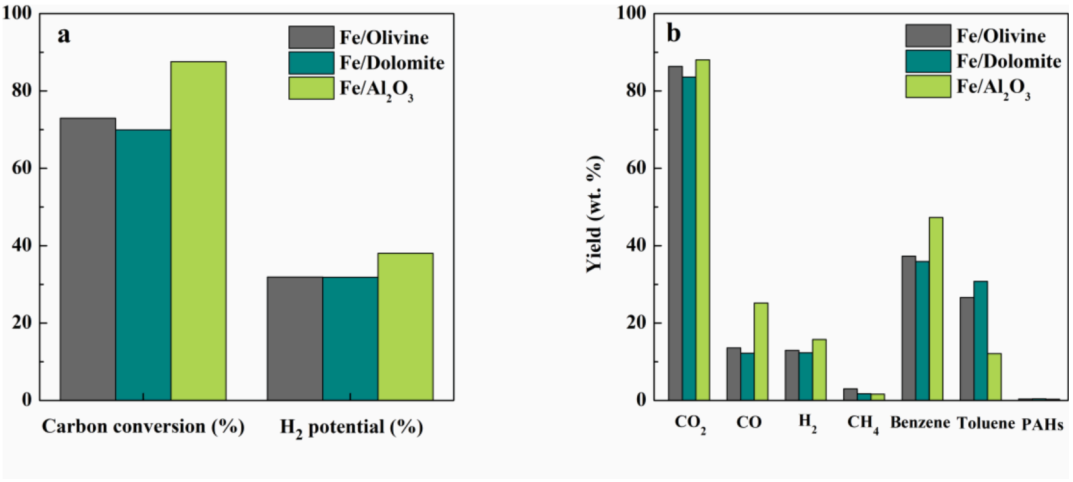

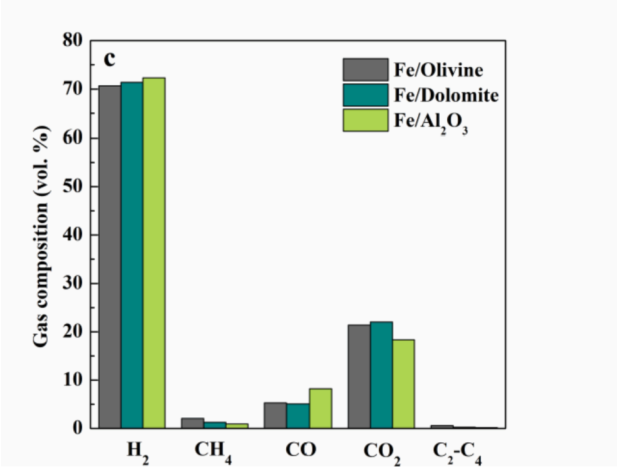

Fig. 6. Effect of Fe impregnated catalysts on carbon conversion and H_2 potential (a), product yields and unreacted toluene fraction in the outlet stream (b), and concentration of gaseous compounds (c).

the active phase, and therefore lead to higher catalyst activity. Besides, the higher dispersion of Fe on olivine also explains the higher carbon conversion than on Fe/dolomite.

Another factor is related to the activity of the support for cracking and/or reforming reactions, which is directly linked to its acidity [30,57]. Thus, the porous structure of olivine and dolomite barely have micro or mesopores, whereas alumina has a more developed porous structure, as shown in Table 1. Adnan et al. [85] suggested that toluene conversion reactivity is dominated by strong acid sites in the catalyst, which are directly attached to the surface of the catalyst. Thus, a higher surface area of the catalyst increases the number of strong sites available to contact with toluene, thereby leading to a higher acidity of the catalysts, and consequently to a higher conversion of toluene, as is the case of Fe/Al_2O_3, which has the highest acidity (Table 1) of the three Fe loaded catalysts [87]. Besides, Adnan et al. [88] stated that a higher content of Fe in the catalyst also promotes catalyst acidity, and therefore toluene conversion. Comparing the acidity of primary and Fe doped catalysts (Table 1), the presence of Fe increases the acidity of Fe/olivine and Fe/dolomite catalysts from 2.4 to 8.8 and from 8.7 to 10.5 μmol NH_3 g_{cat}^{-1}, respectively, which explains the higher toluene cracking capability of Fe doped ones. Regarding the acidity value of Fe/Al_2O_3 (11.4 μmol NH_3 $g_{cat^{-1}}$), it is much lower than that of the raw γ-Al_2O_3. Indeed, as previously stated, the reduction in BET surface area caused by the calcination and impregnation stages leads to the blockage of some pores and reduces the number of acid sites available, thus reducing the total acidity of the catalyst. However, comparing Fig. 5b and 6b, benzene yield is higher when Fe/Al_2O_3 is used than when the primary Al_2O_3 is used, which suggests that the cracking activity of Fe/Al_2O_3 is higher. This result is explained by the combination of two issues. On the one hand, as was previously stated, the better performance of Fe for reforming and WGS reactions leads to higher H_2 partial pressures in the reaction environment, thus promoting hydrodealkylation reactions (Eq. 6) which lead to higher benzene contents. On the other hand, the real acidity of γ-Al_2O_3 under reaction conditions is much lower than that given in Table 1, as the high temperatures used in this study (850 °C) and the presence of steam accelerate the collapse of the porous structure and the transformation of γ-alumina into other more stable phases, as stated elsewhere [47]. Thus, the blockage of pores and the transformation of γ-phase into other ones (δ, θ or α) reduces the number of acid sites available, and therefore its cracking activity.

Other important issue involving catalytic activity is the reduction state of the iron species, with activity being higher as Fe species are further reduced (metal Fe is the most active phase). Thus, the XRD patterns in the three fresh catalysts reveal the presence of metal Fe, whereas the presence of other species with different reduction states, such as Fe_2O_3, Fe_3O_4 or FeO, was not initially observed (Fig. 2b). This is an evidence that the difference in the catalytic activities of Fe impregnated catalysts is mostly attributed to the interactions between the metal iron and the supports, as well as their physical structure. Thus, the better properties of Al_2O_3 (it acts as a textural promoter preventing the fast sintering of the iron metal, as well as stabilizing active sites on its surface) lead to better dispersion of the Fe oxide phase, and therefore better

performance for toluene steam reforming and WGS reaction [38].

Claude et al. [26] analysed the effect of Fe doped olivine and alumina catalysts and revealed that Fe/Al_2O_3 provided also higher toluene conversion than the Fe/olivine catalyst when temperature was 850 °C. Nevertheless, the olivine catalyst was the one of better performance at 750 °C. It should be noted that these authors reduced both catalysts *in situ* in the reactor with an inlet reactant gas mixture containing 31.5 % vol. H_2, which simulates a feed containing a fraction of the reforming outlet stream. Therefore, the differences at this temperature can be explained by the presence of iron species with different reduction states (active for steam reforming) in the olivine, whereas Fe was only present as hercynit in the case of alumina.

3.5. Evaluation of Fe-based catalysts stability

Fig. 7 displays the evolution of carbon conversion and H_2 potential with time on stream in the toluene steam reforming at 850 °C on the three catalyst tested. As observed, Fe/Al_2O_3 provided the highest stability in terms of carbon conversion (Fig. 7a) and H_2 potential (Fig. 7b), since it allowed operating for the longest period with the highest conversion (85.9 % after 35 min on stream). Fe/dolomite and Fe/olivine catalysts provided a rather stable activity for the first 15 min, but the deactivation rate increased greatly subsequent to this time, and therefore toluene conversion and H_2 potential decreased rapidly. The decrease in these parameters in the range from 15 to 25 min is more pronounce on the Fe/dolomite catalyst (35.1 % and 18.0 %, respectively, at the end of 25 min on stream). Subsequent to this time, the Fe/olivine catalyst underwent more severe decrease to 31.0 % and 15.8 %, respectively, after 45 min on stream. Overall, the conversion level and H_2 yield decreased gradually with reaction time when either catalyst was used, reaching similar steady values of around 30 % and 15 %, respectively, which is evidence of the deactivation underwent by the catalysts.

The evolution of component yields in the product stream with reaction time is shown in Fig. 8 for the three Fe doped catalysts. As observed, the yields of toluene and benzene follow opposite trends in the three catalysts. Once the activity for toluene reforming and cracking is low due to catalysts deactivation, the yield of toluene increases, whereas that of benzene decreases. Given the higher activity and stability on the Fe/Al_2O_3 catalyst for a longer time, benzene yield is higher and remains at around 45 wt% for a longer period than on Fe/olivine and Fe/dolomite. However, Fe/Al_2O_3 catalyst deactivation is more pronounced, attaining yields of H_2 and CO lower than 10 wt%. Thus, Fe/dolomite provided lowest yields of toluene and highest of benzene when it was deactivated (65.2 and 14.6 wt%, respectively, for 65 min on stream), which means it is more active for toluene cracking than the other ones subsequent to this time. As previously stated, dolomite is well-known as an active catalyst for tar conversion when it is in the calcined state, i.e., CaO and MgO state, and therefore these species are still active phases for toluene cracking subsequent to the mentioned time [89].

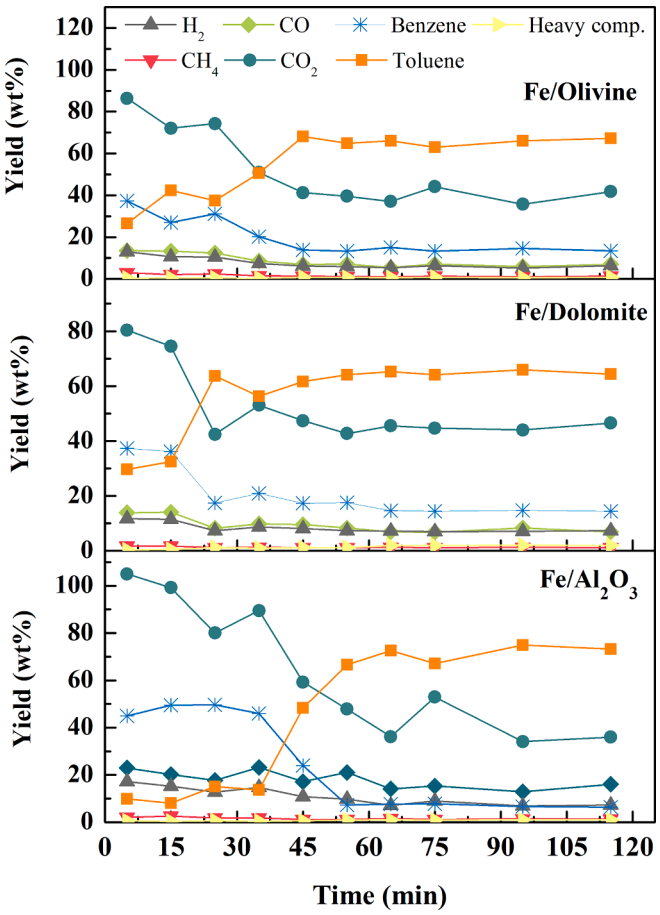

Fig. 8. Evolution of product yields with time on stream for the Fe loaded catalysts.

Moreover, as time on stream increased, H_2 and CO_2 yield decreased for the three catalysts, which is evidence of the lower extension of reforming and WGS reactions when the catalysts undergo deactivation. This reduction is more pronounced in the Fe/Al_2O_3 catalyst, in which the H_2 yield decreased steadily from 17.5 to 7.3 wt% and that of CO_2 from 105.0 to 36.0 wt% for 115 min on stream. These results and those corresponding to benzene and toluene yields confirm that, although the Fe/Al_2O_3 catalyst was able to maintain its reforming/cracking capacity for longer time, the deactivation was more severe.

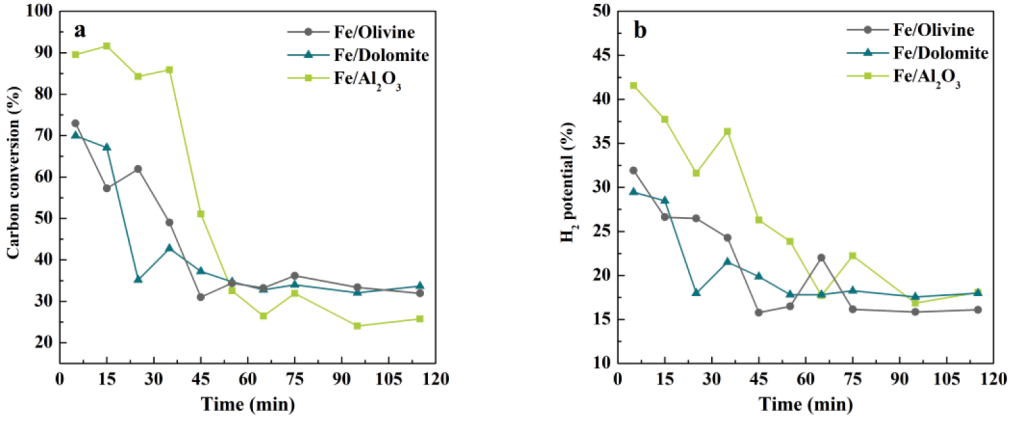

Fig. 7. Evolution of carbon conversion (a) and H_2 potential (b) with time on stream for the three catalysts studied.

Regarding the CO yield, it was almost constant for Fe/Al_2O_3, whereas it decreased slightly for Fe/olivine and Fe/dolomite (from 13.7 to 6.9 wt % on both catalysts), although the latter allows operation for longer time on stream until reaching this final yield. This trend is a consequence of a balance between the attenuation of reforming (Eqs. 1 and 7) and WGS (Eq. 3) reactions and CO formation by mainly decarbonylation (cracking) [90,91].

Regarding CH_4 yields, they decreased slightly as reaction proceeded, attaining a value of around 1.25 wt% in the three catalysts. These results are evidence of the attenuation of the hydrodealkylation reaction (Eq. 6) when deactivation proceeded, although CH_4 may still be formed by the cracking of the hydrocarbons in the reaction environment or by methanation (Eq. 9). A similar explanation holds for the slight increase in the yield of heavier hydrocarbons with time on stream. In this case, the attenuation of hydrocarbon reforming reactions by catalyst deactivation enables hydrocarbon rearrangement reactions, such as polymerization and/or cycloaddition, which lead to higher molecular weight species than toluene [21,92].

The faster deactivation of olivine and dolomite catalysts shown in Figs. 7 and 8 suggests that the role of metal-support interactions, as well as the structural characteristics of the supports, in the metal dispersion may be relevant in the catalyst deactivation mechanism [37]. In fact, the poorer metal dispersion on dolomite and olivine catalysts, and therefore the lower amount of Fe active sites available for reforming and WGS reactions, enhances catalyst deactivation, either by sintering, coke deposition or iron phase change (reduction in metal active sites by the oxidation of iron species). As reported by other researchers, iron is more active for tar cracking/reforming when it is in the metal state than oxidized, but the oxidizing nature of steam at high temperatures promotes the oxidation of Fe metal sites [37,83]. Furthermore, given the lower dispersion of Fe on Fe/olivine and Fe/dolomite catalysts, most of it will be deposited on the catalyst surface, which leads to faster coke deposition, and therefore faster deactivation [24]. In fact, the deactivation mechanism by coking for toluene steam reforming is well established in the literature on Fe based catalysts [58,88]. The deactivation mechanism for the three catalysts will be further discussed in the next section.

3.6. Analysis of catalyst deactivation causes

Prevention and attenuation of catalyst deactivation is essential for improving the viability of this catalytic process at larger scale. Therefore, a detailed characterization of the deactivated catalysts was carried out in order to understand the main causes of catalysts activity decay. Based on the results obtained in this study and others reported in the literature, the main factors causing the deactivation of Fe impregnated catalysts are coke deposition and active phase oxidation. Nevertheless, sintering or iron loss by attrition may also be relevant [22,25,26,62].

Table 3
Physical and chemical properties of the spent catalysts.

	Fe/Olivine	Fe/Al_2O_3	Fe/Dolomite
Physical properties			
S_{BET} ($m^2\ g^{-1}$)	3.02	7.63	3.29
V_{pore} ($cm^3\ g^{-1}$)	0.010	0.044	0.021
d_{pore} (Å)	217	285	388
Chemical properties			
MgO (wt%)	36.39	0.19	29.47
SiO_2 (wt%)	36.23	–	0.11
Fe_2O_3 (wt%)	23.24	13.64	12.16
CaO (wt%)	0.31	0.05	43.48
Al_2O_3 (wt%)	0.63	82.81	0.29
Na_2O (wt%)	0.07	–	0.29
TiO_2 (wt%)	0.03	0.11	0.03
MnO (wt%)	0.10	0.01	–
K_2O (wt%)	0.01	–	–
P_2O_5 (wt%)	–	–	0.01

Table 3 shows the textural properties of deactivated Fe/olivine, Fe/dolomite and Fe/Al_2O_3 catalysts once they were used for 115 min on stream. Comparing these properties with those displayed in Table 1 for fresh catalysts, the BET surface areas remained almost constant for Fe/olivine and Fe/dolomite catalysts, whereas the Fe/Al_2O_3 underwent a reduction from 12.48 in the fresh one to 7.63 $m^2\ g^{-1}$ in the deactivated one. Pore volume and pore diameter of the Fe/olivine catalyst decreased from 0.017 $cm^3\ g^{-1}$ and 234 Å to 0.010 $cm^3\ g^{-1}$ and 217 Å, respectively, thus revealing a partial blockage of the catalyst pores, but not their complete clogging. Moreover, the pore volume also decreased in the deactivated Fe/Al_2O_3, but the pore diameter increased from 206 to 285 Å, which suggests that the smallest pores are fully blocked by coke deposition. Similarly, the pore diameter increased in the spent Fe/dolomite, which reveals blockage or partial obstruction of the smallest pores.

Table 3 also displays the chemical composition of the deactivated catalysts. A comparison of these values with those of the fresh ones (Table 1) allows concluding that there is not significant iron loss by attrition phenomena. Thus, the iron oxide content decreased slightly in the deactivated catalysts, i.e., 3.15 wt% in the Fe/olivine, 0.49 wt% in the Fe/Al_2O_3 and 1.48 wt% in the Fe/dolomite. The absence of attrition

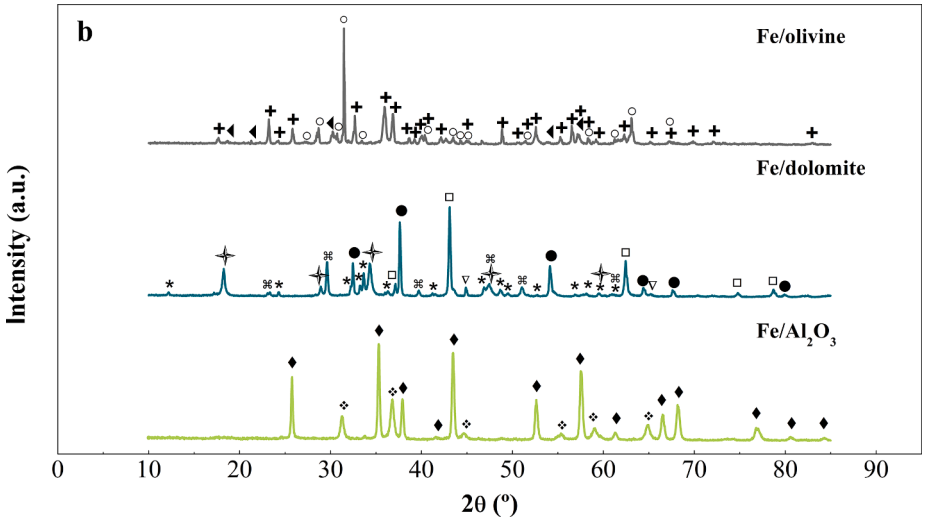

Fig. 9. XRD profiles of the spent Fe/olivine, Fe/dolomite and Fe/Al_2O_3 catalysts. Crystalline phases: (+) ($Mg_{1.81}Fe_{0.19}(SiO_4)$); (o) Enstatite ($MgSiO_3$); (◂) Magnetite ($Fe_3O_4$); (▽) Fe^0; (◆) Al_2O_3; (□) MgO; (●) CaO; (❖) Hercynite ($FeAl_2O_4$); (✦) Calcium hidroxide ($CaOH_2$); (*) Calcium iron oxide ($Ca_2Fe_2O_5$); (⌘) $CaCO_3$.

phenomena was also checked by sieving the deactivated catalysts particles. Thus, their size is approximately the same as the fresh ones, i.e., 90–150 μm for olivine, 150–250 μm for dolomite and 250–400 μm for alumina. The higher loss of Fe in the Fe/olivine and Fe/dolomite catalysts is related to the weaker interaction between the Fe and the support, as the metal species is mainly located on the surface [26]. Overall, these results of XRF analysis reveal that catalyst deactivation is not caused by the loss of metal phase.

Fig. 9 shows the XRD patterns of the spent catalyst, which allow assessing the influence of the active phase oxidation in the deactivation process. As observed, the diffraction lines attributed to metal iron ($2\theta = 45^\circ$ and $2\theta = 65^\circ$) are only present in the Fe/dolomite sample, although their intensity is greatly reduced compared to those of the fresh one (Fig. 2). The XRD profiles for neither Fe/olivine nor Fe/Al_2O_3 contain these lines, which explains the slightly higher activity of Fe/dolomite for toluene reforming and WGS at longer times on stream. Nevertheless, lines for other iron phases have been detected in the three catalysts, with some of them being absent in the diffractograms for the fresh ones. The X-ray pattern of the deactivated Fe/Al_2O_3 only shows the presence of iron strongly incorporated into alumina (hercynite, $FeAl_2O_4$). A new phase of calcium iron oxide ($Ca_2Fe_2O_5$) appears in the Fe/dolomite, which is formed due to the interaction between the metal iron and calcium oxide in the presence of steam [63]. The presence of $Ca_2Fe_2O_5$ (reducible at high temperatures) promoted the redox reaction of Fe^{3+} to Fe^0 due to its great oxygen-carrying capacity, which explains the presence of metal iron in the Fe/dolomite after the steam reforming process [78,93]. Given that MgO-iron oxide is detected, it can be assumed that iron only reacts with CaO, which was also concluded by Di Felice et al. [94]. Note that the spent Fe/dolomite catalyst shows certain decrease in the intensity of MgO and CaO peaks with respect to the fresh one (Fig. 2b), as well as the presence of the calcite phase (not observed in fresh catalyst), probably due to a very limited carbonation at 850 °C in the gasifier. These results confirm that CaO and MgO are still the most important active phases for toluene cracking on the spent catalyst. Concerning the Fe/olivine XRD profile, apart from the $Mg_{1.81}Fe_{0.19}(SiO_4)$ olivine phase previously detected in the fresh catalyst, new Fe_3O_4 lines appear at $2\theta = 18^\circ$, 21°, 30°, 54° and 57°. These new iron phases, together with the absence or sharp reduction in Fe^0 lines, are evidence of a loss of active phase by metal iron oxidation under the reaction conditions used on the three catalysts analysed. However, Fe_3O_4 phase in the Fe/olivine and $Ca_2Fe_2O_5$ in the Fe/dolomite are still active for the reforming and WGS reactions, which explains their slightly higher carbon conversion than Fe/Al_2O_3 when they underwent deactivation (Fig. 7a).

Another cause of catalyst deactivation with time on stream is the coke deposited on these catalysts. Therefore, spent catalysts were subjected to temperature programme oxidation (TPO) in order to assess the amount and nature of the coke deposited. This coke blocks the access of reactants to the metal sites or encapsulates the Fe particles, thereby deactivating the crystallite. The TPO analyses revealed that the highest amount of coke deposits were formed on the Fe/Al_2O_3 catalyst, followed by Fe/olivine and Fe/dolomite, with values being 4.10, 2.36 and 1.17 wt %, respectively. It is well stablished in the literature that the rate and extent of coke formation increases by increasing the acid strength of the catalyst [57,95]. Thus, the higher coke deposition on the Fe/Al_2O_3 catalyst is explained by the higher acidity of alumina than olivine and dolomite. Moreover, the lowest coke formation rate in the Fe/dolomite catalyst is explained by two facts: (i) the presence of $Ca_2Fe_2O_5$ phase (oxygen carrier) improves oxygen mobility on the catalyst surface, and therefore leads to faster carbon removal by oxidation, and (ii) the presence of CaO and MgO in the dolomite favours steam-carbon reactions, thus hindering polymerization reactions that promote coke development [89]. However, it should be noted that the catalytic activity of CaO for steam reforming decreases dramatically when the carbonate is formed [96]. Zamboni et al. [63] suggested that the oxygen vacancies in the $Ca_2Fe_2O_5$ structure favour the reduction of water and, furthermore, $Ca_2Fe_2O_5$ rearranges by releasing oxygen, which oxidizes carbon species to CO_2. Note that the CO_2 yield (45.5 wt%) is the highest on the Fe/dolomite, even though the H_2 yield is similar in the product stream once catalysts have been deactivated (Fig. 8).

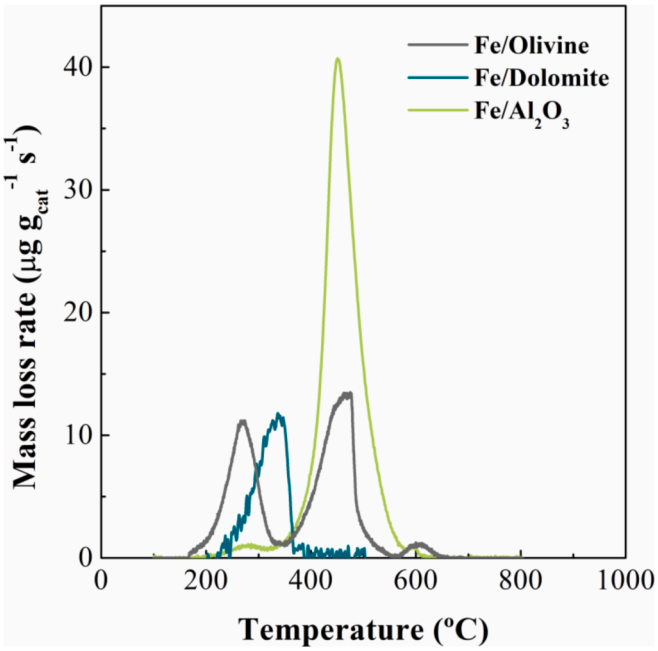

Fig. 10. TPO profiles of the spent catalysts.

Fig. 10 displays the TPO profiles of the spent catalysts, which allow determining the nature and the possible location of the coke within the catalyst. Apart from the mentioned differences in the amount of coke deposited, Fig. 10 shows that the nature of the coke varies depending on the type of support. A prevailing peak is observed at 450 °C for Fe/olivine and Fe/Al_2O_3, which is related to the combustion of the amorphous coke (hydrogenated composition) deposited on metal particles. Two small peaks are also observed at 600 °C for these catalysts, which are related to a more structured coke located on the catalyst support, even though its content is almost negligible due to the low intensity of both peaks. Another oxidation peak was detected at around 270 °C for the Fe/olivine catalyst, which is related to a less structured coke or heavy hydrocarbon deposits [37]. Virginie et al. [24] also detected 3 peaks in the TPO of a 10 wt% Fe/olivine deactivated catalyst. The first one at around 360 °C, which is attributed to surface carbon oxidation, the second one at around 500 °C, which is due to the oxidation of iron carbide, and the third one at around 610 °C assigned to filamentous carbon oxidation. The Fe/dolomite catalyst seemed to be more effective than the other two catalysts for preventing coke formation and, furthermore, its coke burns at lower temperatures (the main peak below 400 °C). This is explained by the presence of $Ca_2Fe_2O_5$ phase, which increases oxygen mobility on the catalysts surface, thus favouring coke gasification and inhibiting its growth and evolution towards a more structured coke [93].

In view of these results, it may be concluded that the active phase oxidation is the main deactivation cause, but the coke deposited on the Fe active sites also causes their blockage, and therefore contributes to the catalysts deactivation. The deactivation of Fe/dolomite and Fe/olivine catalysts is faster because the iron is mainly located on the external surface, and therefore coking reactions encapsulate more easily the metal particles. Indeed, the surface area of olivine and dolomite supports is limited, and therefore Fe dispersion is more restrictive than in the alumina support. The latter undergoes more severe deactivation by coke deposition, but this occurs for longer reaction periods.

4. Conclusions

This study approaches tar elimination by feeding toluene as a representative tar compound and shows that Fe incorporation into olivine, dolomite and alumina increases the activity and selectivity towards hydrocarbon reforming and WGS reactions. The results are evidence that an increase in temperature to 900 °C leads to an increase in carbon conversion and H_2 potential due to the enhancement of toluene reforming and cracking reactions. Concerning the efficiency of the primary catalysts, alumina provides the highest carbon conversion followed by dolomite, with their H_2 potential being similar. In fact, the higher acidity of alumina promotes catalytic cracking reactions, thus leading to higher carbon conversions, even though its activity for WGS reaction is more limited. Dolomite is the one of highest activity for WGS reactions, which is related to CaO and MgO basic sites obtained after calcination. In addition, the presence of these species also improves tar decomposition, which in turn increases benzene yield at the expense of decreasing that of toluene.

Regarding Fe loaded catalysts, Fe/Al_2O_3 provides the best performance in terms of carbon conversion and H_2 potential. In fact, the higher porosity and BET surface area of alumina compared to those of olivine and dolomite improves the dispersion of Fe, which acts as the active phase for reforming and WGS reactions, whereas the alumina support provides the acidity required for cracking reactions. Furthermore, Fe/Al_2O_3 is the most stable catalyst and allows operating for longer periods with higher conversion values, whereas Fe/olivine, and especially Fe/dolomite, undergo faster deactivation, as evidenced by the sharper decrease in the reaction indices.

The analyses of spent catalysts show that the main deactivation cause is the active phase oxidation followed by coke deposition on Fe active sites during the toluene conversion process. The XRD patterns show new iron oxidized phases and the absence of Fe^0 lines (except for Fe/dolomite, with their intensity being significantly lower than those of the fresh one), whereas TPO analyses reveal a higher coke deposition for Fe/Al_2O_3 (4.4 wt%), which fully blocks the smallest pores of the catalyst. The coke deposited in all the spent catalysts has an amorphous nature and blocks the access of reactants to the metal sites, thereby deactivating the catalysts.

CRediT authorship contribution statement

Maria Cortazar: Investigation, Data curation, Methodology. **Jon Alvarez:** Writing – original draft, Writing – review & editing, Formal analysis, Visualization. **Leire Olazar:** Investigation, Data curation. **Laura Santamaria:** Validation, Data curation. **Gartzen Lopez:** Conceptualization, Methodology, Supervision. **Heidi Isabel Villafán-Vidales:** Methodology, Validation. **Asier Asueta:** Supervision. **Martin Olazar:** Supervision, Conceptualization, Writing – review & editing, Project administration.

Declaration of Competing Interest

The authors declare that they have no known competing financial interests or personal relationships that could have appeared to influence the work reported in this paper.

Acknowledgments

This work was carried out with the financial support of the grants RTI2018-098283-J-I00 and PID2019−107357RB-I00 funded by MCIN/AEI/ 10.13039/501100011033 and by "ERDF A way of making Europe" and the grants IT1218−19 and KK-2020/00107 funded by the Basque Government. Moreover, this project has received funding from the European Union's Horizon 2020 research and innovation programme under the Marie Sklodowska-Curie grant agreement No 823745.

References

[1] Yu J, Guo Q, Gong Y, Ding L, Wang J, Yu G. A review of the effects of alkali and alkaline earth metal species on biomass gasification. Fuel Process Technol 2021; 214:106723. https://doi.org/10.1016/j.fuproc.2021.106723.
[2] Larsson A, Kuba M, Berdugo Vilches T, Seemann M, Hofbauer H, Thunman H. Steam gasification of biomass – Typical gas quality and operational strategies derived from industrial-scale plants. Fuel Process Technol 2021;212:106609. https://doi.org/10.1016/j.fuproc.2020.106609.
[3] Swierczynski D, Courson C, Kiennemann A. Study of steam reforming of toluene used as model compound of tar produced by biomass gasification. Chem Eng Process 2008;47:508–13. https://doi.org/10.1016/j.cep.2007.01.012.
[4] Ren J, Cao J, Zhao X, Liu Y. Fundamentals and applications of char in biomass tar reforming. Fuel Process Technol 2021;216:106782. https://doi.org/10.1016/j.fuproc.2021.106782.
[5] Casari N, Pinelli M, Suman A, Candido A, Morini M. Deposition of syngas tar in fuel supplying duct of a biomass gasifier: A numerical study. Fuel 2020;273:117579. https://doi.org/10.1016/j.fuel.2020.117579.
[6] Lepage T, Kammoun M, Schmetz Q, Richel A. Biomass-to-hydrogen: A review of main routes production, processes evaluation and techno-economical assessment. Biomass Bioenergy 2021;144:105920. https://doi.org/10.1016/j.biombioe.2020.105920.
[7] Lu M, Xiong Z, Li J, Li X, Fang K, Li T. Catalytic steam reforming of toluene as model tar compound using Ni/coal fly ash catalyst. Asia-Pac J Chem Eng 2020. https://doi.org/10.1002/apj.2529.
[8] Artetxe M, Alvarez J, Nahil MA, Olazar M, Williams PT. Steam reforming of different biomass tar model compounds over Ni/Al2O3 catalysts. Energy Convers Manage 2017;136:119–26. https://doi.org/10.1016/j.enconman.2016.12.092.
[9] Li C, Suzuki K. Tar property, analysis, reforming mechanism and model for biomass gasification—An overview. Renew Sustain Energ Rev 2009;13:594–604. https://doi.org/10.1016/j.rser.2008.01.009.
[10] Meng J, Wang X, Zhao Z, Wu X, Zheng A, Wei G, et al. A highly carbon-resistant olivine thermally fused with metallic nickel catalyst for steam reforming of biomass tar model compound. RSC Adv 2017;7:39160–71. https://doi.org/10.1039/C7RA06219B.
[11] Abou Rached J, El Hayek C, Dahdah E, Gennequin C, Aouad S, et al. Ni based catalysts promoted with cerium used in the steam reforming of toluene for hydrogen production. Int J Hydrogen Energy 2017;42:12829–40. https://doi.org/10.1016/j.ijhydene.2016.10.053.
[12] Belbessai S, Achouri IE, Benyoussef EH, Gitzhofer F, Abatzoglou N. Toluene steam reforming using nickel based catalysts made from mining residues. Catal Today 2020;36:111–21. https://doi.org/10.1016/j.cattod.2020.07.087.
[13] Sayas S, Vivó N, Da Costa-Serra JF, Chica A. Toluene steam reforming over nickel based catalysts. Int J Hydrogen Energy 2021;46:17472-80 10.1016/j.ijhydene.2020.04.235.
[14] Guan G, Kaewpanha M, Hao X, Abudula A. Catalytic steam reforming of biomass tar: Prospects and challenges. Renew Sustain Energ Rev 2016;58:450–61. https://doi.org/10.1016/j.rser.2015.12.316.
[15] Oemar U, Ming Li A, Hidajat K, Kawi S. Mechanism and kinetic modeling for steam reforming of toluene on La0.8Sr0.2Ni0.8Fe0.2O3 catalyst. AIChE J 2014;60: 4190–8. https://doi.org/10.1002/aic.14573.
[16] Xu M, Hu H, Yang F, Yang Y, Jiang L, Tang H, et al. Novel findings in conversion mechanism of toluene as model compound of biomass waste tar in molten salt. J Anal Appl Pyrolysis 2018;134:274–80. https://doi.org/10.1016/j.jaap.2018.06.017.
[17] D'Orazio A, Di Carlo A, Dionisi N, Dell'Era A, Orecchini F. Toluene steam reforming properties of CaO based synthetic sorbents for biomass gasification process. Int J Hydrogen Energy 2013;38:13282–92. https://doi.org/10.1016/j.ijhydene.2013.07.075.
[18] Josuinkas FM, Quitete CPB, Ribeiro NFP, Souza MMVM. Steam reforming of model gasification tar compounds over nickel catalysts prepared from hydrotalcite precursors. Fuel Process Technol 2014;121:76–82. https://doi.org/10.1016/j.fuproc.2014.01.007.
[19] Ashok J, Dewangan N, Das S, Hongmanorom P, Wai MH, Tomishige K, et al. Recent progress in the development of catalysts for steam reforming of biomass tar model reaction. Fuel Process Technol 2020;199:106252. https://doi.org/10.1016/j.fuproc.2019.106252.
[20] Valderrama Rios ML, González AM, Lora EES, Almazán del Olmo OA. Reduction of tar generated during biomass gasification: A review. Biomass Bioenergy 2018;108: 345–70. https://doi.org/10.1016/j.biombioe.2017.12.002.
[21] Cortazar M, Alvarez J, Lopez G, Amutio M, Santamaria L, Bilbao J, et al. Role of temperature on gasification performance and tar composition in a fountain enhanced conical spouted bed reactor. Energy Convers Manage 2018;171: 1589–97. https://doi.org/10.1016/j.enconman.2018.06.071.
[22] Cortazar M, Santamaria L, Lopez G, Alvarez J, Amutio M, Bilbao J, et al. Fe/olivine as primary catalyst in the biomass steam gasification in a fountain confined spouted bed reactor. J Ind Eng Chem 2021;99:364–79. https://doi.org/10.1016/j.jiec.2021.04.046.
[23] Richardson Y, Blin J, Julbe A. A short overview on purification and conditioning of syngas produced by biomass gasification: Catalytic strategies, process intensification and new concepts. Prog Energy Combust Sci 2012;38:765–81. https://doi.org/10.1016/j.pecs.2011.12.001.
[24] Virginie M, Courson C, Niznansky D, Chaoui N, Kiennemann A. Characterization and reactivity in toluene reforming of a Fe/olivine catalyst designed for gas cleanup in biomass gasification. Appl Catal B Environ 2010;101:90–100. https://doi.org/10.1016/j.apcatb.2010.09.011.

[25] Virginie M, Adánez J, Courson C, et al. Effect of Fe–olivine on the tar content during biomass gasification in a dual fluidized bed. Appl Catal B Environ 2012; 121–122:214–22. https://doi.org/10.1016/j.apcatb.2012.04.005.
[26] Claude V, Mahy JG, Douven S, Pirard SL, Courson C, Lambert SD. Ni- and Fe-doped γ-Al2O3 or olivine as primary catalyst for toluene reforming. Mater Today Chem 2019;14:100197. https://doi.org/10.1016/j.mtchem.2019.100197.
[27] Ashok J, Kathiraser Y, Ang ML, Kawi S. Bi-functional hydrotalcite-derived NiO–CaO–Al2O3 catalysts for steam reforming of biomass and/or tar model compound at low steam-to-carbon conditions. Appl Catal B 2015;172–173:116–28. https://doi.org/10.1016/j.apcatb.2015.02.017.
[28] Ashok J, Kawi S. Steam reforming of biomass tar model compound at relatively low steam-to-carbon condition over CaO-doped nickel-iron alloy supported over iron-alumina catalysts. Appl Catal A Gen 2015;490:24–35. https://doi.org/10.1016/j.apcata.2014.10.057.
[29] Li S, Gong J. Strategies for improving the performance and stability of Ni-based catalysts for reforming reactions. Chem Soc Rev 2014;43:7245–56. https://doi.org/10.1039/C4CS00223G.
[30] Chan FL, Tanksale A. Review of recent developments in Ni-based catalysts for biomass gasification. Renewable Sustain Energy Rev 2014;38:428–38. https://doi.org/10.1016/j.rser.2014.06.011.
[31] Sayas S, Chica A. Furfural steam reforming over Ni-based catalysts. Influence of Ni incorporation method. Int J Hydrogen Energy 2014;39:5234–41. https://doi.org/10.1016/j.ijhydene.2014.01.115.
[32] Kumagai S, Alvarez J, Blanco PH, Wu C, Yoshioka T, Olazar M, et al. Novel Ni-Mg-Al-Ca catalyst for enhanced hydrogen production for the pyrolysis-gasification of a biomass/plastic mixture. J Anal Appl Pyrolysis 2015;113:15–21. https://doi.org/10.1016/j.jaap.2014.09.012.
[33] Alvarez J, Kumagai S, Wu C, Yoshioka T, Bilbao J, Olazar M, et al. Hydrogen production from biomass and plastic mixtures by pyrolysis-gasification. Int J Hydrogen Energy 2014;39:10883–91. https://doi.org/10.1016/j.ijhydene.2014.04.189.
[34] Michel R, Łamacz A, Krzton A, Djéga-Mariadassou G, Burg F, Courson C, et al. Steam reforming of α-methylnaphthalene as a model tar compound over olivine and olivine supported nickel. Fuel 2013;109:653–60. https://doi.org/10.1016/j.fuel.2013.03.017.
[35] Santamaria L, Lopez G, Fernandez E, Cortazar M, Arregi A, Olazar M, et al. Progress on Catalyst Development for the Steam Reforming of Biomass and Waste Plastics Pyrolysis Volatiles: A Review. Energy Fuels 2021. https://doi.org/10.1021/acs.energyfuels.1c01666.
[36] Pfeifer C, Rauch R, Hofbauer H. In-Bed Catalytic Tar Reduction in a Dual Fluidized Bed Biomass Steam Gasifier. Ind Eng Chem Res 2004;43:1634–40. https://doi.org/10.1021/ie030742b.
[37] Yang S, Zhang X, Chen L, Sun L, Zhao B, Si H, et al. Pyrolysis of sawdust with various Fe-based catalysts: Influence of support characteristics on hydrogen-rich gas production. J Anal Appl Pyrolysis 2019;137:29–36. https://doi.org/10.1016/j.jaap.2018.10.021.
[38] Zhu M, Wachs IE. Iron-Based Catalysts for the High-Temperature Water-Gas Shift (HT-WGS) Reaction: A Review. ACS Catal 2016;6:722–32. https://doi.org/10.1021/acscatal.5b02594.
[39] Chou C, Loiland JA, Lobo RF. Reverse Water-Gas Shift Iron Catalyst Derived from Magnetite. Catalysts 2019;9:773. https://doi.org/10.3390/catal9090773.
[40] Baraj E, Ciahotný K, Hlinčík T. The water gas shift reaction: Catalysts and reaction mechanism. Fuel 2021;288:119817. https://doi.org/10.1016/j.fuel.2020.119817.
[41] Anis S, Zainal ZA. Tar reduction in biomass producer gas via mechanical, catalytic and thermal methods: A review. Renewable Sustain Energy Rev 2011;15:2355–77. https://doi.org/10.1016/j.rser.2011.02.018.
[42] Cortazar M, Lopez G, Alvarez J, Amutio M, Bilbao J, Olazar M. Advantages of confining the fountain in a conical spouted bed reactor for biomass steam gasification. Energy 2018;153:455–63. https://doi.org/10.1016/j.energy.2018.04.067.
[43] Cortazar M, Lopez G, Alvarez J, Amutio M, Bilbao J, Olazar M. Behaviour of primary catalysts in the biomass steam gasification in a fountain confined spouted bed. Fuel 2019;253:1446–56. https://doi.org/10.1016/j.fuel.2019.05.094.
[44] Arregi A, Abbas-Abadi MS, Lopez G, Santamaria L, Artetxe M, Bilbao J, et al. CeO2 and La2O3 promoters in the steam reforming of polyolefinic waste plastic pyrolysis volatiles on Ni-based catalysts. ACS Sustainable Chem Eng 2020;8:17307–21. https://doi.org/10.1021/acssuschemeng.0c06800.
[45] Wang L, Li D, Koike M, Nakawaga Y, Xu Y, Tomishige K. Catalytic performance and characterization of Ni-Fe catalysts for the steam reforming of tar from biomass pyrolysis to synthesis gas. Appl Catal A Gen 2011;392:248–55. https://doi.org/10.1016/j.apcata.2010.11.013.
[46] Koike M, Li D, Watanabe H, Nakagawa Y, Tomishige K. Comparative study on steam reforming of model aromatic compounds of biomass tar over Ni and Ni–Fe alloy nanoparticles. Appl Catal A Gen 2015;506:151–62. https://doi.org/10.1016/j.apcata.2015.09.007.
[47] Kumar KP, Tranto J, Kumar J, Engell JE. Pore-structure stability and phase transformation in pure and M-doped (M = La, Ce, Nd, Gd, Cu, Fe) alumina membranes and catalyst supports. J Mater Sci Lett 1996;15:266–70. https://doi.org/10.1007/BF00274471.
[48] García-García I, Acha E, Bizkarra K. Martínez de Ilarduya J, Requies J, Cambra JF Hydrogen production by steam reforming of m-cresol, a bio-oil model compound, using catalysts supported on conventional and unconventional supports. Int J Hydrogen Energy 2015;40:14445–55. https://doi.org/10.1016/j.ijhydene.2015.07.155.
[49] Santamaria L, Lopez G, Arregi A, et al. Stability of different Ni supported catalysts in the in-line steam reforming of biomass fast pyrolysis volatiles. Appl Catal B 2019;242:109–20. https://doi.org/10.1016/j.apcatb.2018.09.081.
[50] Santamaria L, Lopez G, Arregi A, Amutio M, Artetxe M, Bilbao J, et al. Influence of the support on Ni catalysts performance in the in-line steam reforming of biomass fast pyrolysis derived volatiles. Appl Catal B Environ 2018;229:105–13. https://doi.org/10.1016/j.apcatb.2018.02.003.
[51] Zhong X, Xie W, Wang N, Duan Y, Shang R, Huang L. Dolomite-derived Ni-based catalysts with Fe modification for hydrogen production via auto-thermal reforming of acetic acid. Catalysts 2016;6:85 10.3390/catal6060085.
[52] Jang W, Jeong D, Shim J, Kim HM, Han WB, Bae JW. Metal oxide (MgO, CaO, and La2O3) promoted Ni-Ce0.8Zr0.2O2 catalysts for H2 and CO production from two major greenhouse gases. Renew. Energy 2015;79:91–5. https://doi.org/10.1016/j.renene.2014.08.032.
[53] Zhou L, Enakonda LR, Saih Y, Loptain S, Gary D, Del Gallo P, et al. Catalytic Methane Decomposition over Fe-Al2 O3. ChemSusChem 2016;9:1243–8. https://doi.org/10.1002/cssc.201600310.
[54] Sarkar R. Sohn HY Interaction of ferrous oxide with alumina refractory under flash ironmaking conditions. Ceram Int 2019;45:15417–28. https://doi.org/10.1016/j.ceramint.2019.05.040.
[55] Lee JS, Kim HS, Park N, Lee TJ, Kang M. Low temperature synthesis of α-alumina from aluminum hydroxide hydrothermally synthesized using [Al(C2O4)x(OH)y] complexes. Chem Eng J 2013;230:351–60. https://doi.org/10.1016/j.cej.2013.06.099.
[56] Ates M, Demir V, Arslan Z, Daniels J, Farah IO, Bogatu C. Evaluation of alpha and gamma aluminum oxide nanoparticle accumulation, toxicity, and depuration in Artemia salina larvae. Environ Toxicol 2015;30:109–18. https://doi.org/10.1002/tox.21917.
[57] Argyle MD, Bartholomew CH. Heterogeneous catalyst deactivation and regeneration: A review. Catalysts 2015;5:145–269. https://doi.org/10.3390/catal5010145.
[58] Virginie M, Courson C, Kiennemann A. Toluene steam reforming as tar model molecule produced during biomass gasification with an iron/olivine catalyst. C R Chim 2010;13:1319–25. https://doi.org/10.1016/j.crci.2010.03.022.
[59] Quan C, Xu S. Zhou C Steam reforming of bio-oil from coconut shell pyrolysis over Fe/olivine catalyst. Energy Convers Manage 2017;141:40–7. https://doi.org/10.1016/j.enconman.2016.04.024.
[60] Zieliński J, Zglinicka I, Znak L, Kaszkur Z. Reduction of Fe2O3 with hydrogen. Appl Catal A Gen 2010;381:191–6. https://doi.org/10.1016/j.apcata.2010.04.003.
[61] Wei X, Zhou Y, Li Y, Shen W. Polymorphous transformation of rod-shaped iron oxides and their catalytic properties in selective reduction of NO by NH3. RSC Adv 2015;5:66141–6. https://doi.org/10.1039/C5RA08254D.
[62] Meng J, Zhao Z, Wang X, Wu X, Zheng A, Huang Z, et al. Effects of catalyst preparation parameters and reaction operating conditions on the activity and stability of thermally fused Fe-olivine catalyst in the steam reforming of toluene. Int J Hydrogen Energy 2018;43:127–38. https://doi.org/10.1016/j.ijhydene.2017.11.037.
[63] Zamboni I, Courson C, Kiennemann A. Fe-Ca interactions in Fe-based/CaO catalyst/sorbent for CO2 sorption and hydrogen production from toluene steam reforming. Appl Catal B 2017;203:154–65. https://doi.org/10.1016/j.apcatb.2016.10.024.
[64] Zamboni I, Courson C, Kiennemann A. Synthesis of Fe/CaO active sorbent for CO2 absorption and tars removal in biomass gasification. Catal Today 2011;176:197–201. https://doi.org/10.1016/j.cattod.2011.01.014.
[65] Giecko G, Borowiecki T, Gac W. Kruk J Fe2O3/Al2O3 catalysts for the N2O decomposition in the nitric acid industry. Catal Today 2008;137:403–9. https://doi.org/10.1016/j.cattod.2008.02.008.
[66] Michorczyk P, Kuśtrowski P, Chmielarz L, Ogonowski J. Influence of redox properties on the activity of iron oxide catalysts in dehydrogenation of propane with CO2. React Kinet Catal Lett 2004;82:121–30. https://doi.org/10.1023/B:REAC.0000028813.14758.ea.
[67] Mosallanejad S, Dlugogorski BZ, Kennedy EM, Stockenhuber M. On the Chemistry of Iron Oxide Supported on γ-Alumina and Silica Catalysts. ACS Omega 2018;3:5362–74. https://doi.org/10.1021/acsomega.8b00201.
[68] Artetxe M, Nahil MA, Olazar M, Williams PT. Steam reforming of phenol as biomass tar model compound over Ni/Al2O3 catalyst. Fuel 2016;184:629–36. https://doi.org/10.1016/j.fuel.2016.07.036.
[69] Kuhn JN, Zhao Z, Felix LG, Slimane RB, Choi CW, Ozkan US. Olivine catalysts for methane- and tar-steam reforming. Appl Catal B Environ 2008;81:14–26. https://doi.org/10.1016/j.apcatb.2007.11.040.
[70] Du Z, Zhang Z, Xu C, Wang X, Li W. Low-Temperature Steam Reforming of Toluene and Biomass Tar over Biochar-Supported Ni Nanoparticles. ACS Sustainable Chem Eng 2019;7:3111–9. https://doi.org/10.1021/acssuschemeng.8b04872.
[71] Iida H, Deguchi S, Torigai M, Osawa Y. Steam reforming of toluene over Ru/SrCO3-Al2O3 catalyst under extremely low steam-to-carbon ratio conditions. Fuel 2020;272:117703. https://doi.org/10.1016/j.fuel.2020.117703.
[72] Morin M, Nitsch X, Pécate S, Hémati M. Tar conversion over olivine and sand in a fluidized bed reactor using toluene as model compound. Fuel 2017;209:25–34. https://doi.org/10.1016/j.fuel.2017.07.084.
[73] Nguyen HNT, Seemann M, Thunman H. Fate of Polycyclic Aromatic Hydrocarbons during Tertiary Tar Formation in Steam Gasification of Biomass. Energy Fuels 2018;32:3499–509. https://doi.org/10.1021/acs.energyfuels.7b03558.
[74] Zhu HL, Pastor-Pérez L, Millan M. Catalytic steam reforming of toluene: Understanding the influence of the main reaction parameters over a reference catalyst. Energies 2020;13:813. https://doi.org/10.3390/en13040813.

[75] Shen Y, Yoshikawa K. Recent progresses in catalytic tar elimination during biomass gasification or pyrolysis—A review. Renew Sustain Energy Rev 2013;21:371–92. https://doi.org/10.1016/j.rser.2012.12.062.
[76] Islam MW. A review of dolomite catalyst for biomass gasification tar removal. Fuel 2020;267:117095. https://doi.org/10.1016/j.fuel.2020.117095.
[77] Quitete CPB, Souza MMVM. Application of Brazilian dolomites and mixed oxides as catalysts in tar removal system. Appl Catal A Gen 2017;536:1–8. https://doi.org/10.1016/j.apcata.2017.02.014.
[78] Xu T, Xu F, Moyo GG, Sun Y, Chen Z, Xiao B, et al. Comparative study of MxOy (M = Cu, Fe and Ni) supported on dolomite for syngas production via chemical looping reforming with toluene. Energy Convers Manage 2019;199:111937. https://doi.org/10.1016/j.enconman.2019.111937.
[79] de Andrés JM, Narros A, Rodríguez ME. Behaviour of dolomite, olivine and alumina as primary catalysts in air–steam gasification of sewage sludge. Fuel 2011; 90:521–7. https://doi.org/10.1016/j.fuel.2010.09.043.
[80] Nam S, Park Y, Yun Y, Gu J, Sung H. Horio M Catalytic application of metallic iron from the dyeing sludge ash for benzene steam reforming reaction in tar emitted from biomass gasification. Korean J Chem Eng 2016;33:465–72. https://doi.org/10.1007/s11814-015-0159-y.
[81] Fredriksson HOA, Lancee RJ, Thüne PC, Veringa HJ, Niemantsverdriet JW. Olivine as tar removal catalyst in biomass gasification: Catalyst dynamics under model conditions. Appl Catal B Environ 2013;130–131:168–77. https://doi.org/10.1016/j.apcatb.2012.10.017.
[82] Ruivo LCM, Pio DT, Yaremchenko AA, Tarelho LAC, Frade JR, Kantarelis E, et al. Iron-based catalyst (Fe2-xNixTiO5) for tar decomposition in biomass gasification. Fuel 2021;300:120859. https://doi.org/10.1016/j.fuel.2021.120859.
[83] Nordgreen T, Liliedahl T, Sjöström K. Metallic iron as a tar breakdown catalyst related to atmospheric, fluidised bed gasification of biomass. Fuel 2006;85:689–94. https://doi.org/10.1016/j.fuel.2005.08.026.
[84] Damma D, Smirniotis PG. Recent advances in iron-based high-temperature water-gas shift catalysis for hydrogen production. Curr Opin Chem Eng 2018;21:103–10. https://doi.org/10.1016/j.coche.2018.09.003.
[85] Adnan MA, Hidayat A, Ajumobi OO, Adamu S, Muraza O, Hossain MM. Fluidizable Fe-Co/Ce-ZrO 2 Catalysts for Steam Reforming of Toluene as a Tar Surrogate in Biomass Gasification. Energy Fuels 2018;32:12833–42. https://doi.org/10.1021/acs.energyfuels.8b02989.
[86] Adnan MA, Adamu S, Muraza O, Hossain MM. Fluidizable NiO–Fe2O3/SiO2–ΓAl2O3 for tar (toluene) conversion in biomass gasification. Process Saf Environ Prot 2018;116:754–62. https://doi.org/10.1016/j.psep.2017.12.021.
[87] Chen G, Liu C, Ma W, Yan B, Ji N. Catalytic Cracking of Tar from Biomass Gasification over a HZSM-5-Supported Ni-MgO Catalyst. Energy Fuels 2015;29: 7969–74. https://doi.org/10.1021/acs.energyfuels.5b00830.
[88] Adnan MA, Muraza O, Razzak SA, Hossain MM, De Lasa HI. Iron Oxide over Silica-Doped Alumina Catalyst for Catalytic Steam Reforming of Toluene as a Surrogate Tar Biomass Species. Energy Fuels 2017;31:7471–81. https://doi.org/10.1021/acs.energyfuels.7b01301.
[89] Gusta E, Dalai AK, Uddin MA, Sasaoka E. Catalytic decomposition of biomass tars with dolomites. Energy Fuels 2009;23:2264–72. https://doi.org/10.1021/ef8009958.
[90] Santamaria L, Artetxe M, Lopez G, et al. Effect of CeO2 and MgO promoters on the performance of a Ni/Al2O3 catalyst in the steam reforming of biomass pyrolysis volatiles. Fuel Process Technol 2020;198:106223. https://doi.org/10.1016/j.fuproc.2019.106223.
[91] Santamaria L, Lopez G, Arregi A, Cortazar M, Amutio M, Bilbao J, et al. Catalytic steam reforming of biomass fast pyrolysis volatiles over Ni–Co bimetallic catalysts. J Ind Eng Chem 2020;91:167–81. https://doi.org/10.1016/j.jiec.2020.07.050.
[92] Rakesh N, Dasappa S. A critical assessment of tar generated during biomass gasification - Formation, evaluation, issues and mitigation strategies. Renew Sustain Energy Rev 2018;91:1045–64. https://doi.org/10.1016/j.rser.2018.04.017.
[93] Sun Z, Chen S, Hu J, Chen A, Rony AH, Russel CK, et al. Ca2Fe2O5: A promising oxygen carrier for CO/CH4 conversion and almost-pure H2 production with inherent CO2 capture over a two-step chemical looping hydrogen generation process. Appl Energy 2018;211:431–42. https://doi.org/10.1016/j.apenergy.2017.11.005.
[94] Di Felice L, Courson C, Niznansky D, Foscolo PU, Kiennemann A. Biomass gasification with catalytic tar reforming: A model study into activity enhancement of calcium- and magnesium-oxide-based catalytic materials by incorporation of iron. Energy Fuels 2010;24:4034–45. https://doi.org/10.1021/ef100351j.
[95] Bartholomew CH. Mechanisms of catalyst deactivation. Appl Catal A Gen 2001; 212:17–60. https://doi.org/10.1016/S0926-860X(00)00843-7.
[96] Shuai C, Hu S, He L, Xiang J, Su S, Sun L, et al. Performance of CaO for phenol steam reforming and water–gas shift reaction impacted by carbonation process. Int J Hydrogen Energy 2015;40:13314–22. https://doi.org/10.1016/j.ijhydene.2015.07.167.